PERGAMON

International Journal of Solids and Structures 36 (1999) 391–425

INTERNATIONAL JOURNAL OF SOLIDS and STRUCTURES

Inelastic deformation and localization in polycarbonate under tension

J. Lu, K. Ravi-Chandar*

Department of Mechanical Engineering, University of Houston, Houston, TX 77204-4792, U.S.A.

Received 20 March 1997; in revised form 1 December 1997

Abstract

It is demonstrated that uniaxial tension deformation in polycarbonate and other polymers that exhibit large inelastic deformation is unstable beyond a certain stretch. The instability first appears as a shear banding phenomenon at a characteristic angle and is then followed by a stabilized neck generation and propagation. The intrinsic material law for polycarbonate is used in a numerical implementation to reproduce completely the deformation behavior observed in uniaxial tension. In particular, it is demonstrated through numerical simulations, that intrinsic material softening is not necessary for the formation of a shear band and continued growth of a stable neck and further that the interpretation of the tensile response in terms of the constitutive behavior of the material poses significant problems.

1. Introduction

Many thermoplastic polymers undergo a significant amount of inelastic deformation prior to failure. This capacity for inelastic deformation is typically exploited in industrial processes such as extrusion, drawing, etc. In order to achieve a predictive capacity for designing such operations, it is necessary to know the constitutive behavior of the material. A major source of problems in characterizing the inelastic constitutive behavior of these materials is the fact that homogeneous deformations are not stable beyond a certain strain level in the most commonly employed experimental configurations such as uniaxial tension and compression, torsion, and simple shear. Localized deformation bands that seem to be a characteristic feature of inelastic deformations develop in each of these experimental configurations; the onset of localization effectively prevents simple evaluation of the experimental results in terms of the constitutive behavior of the material. One must resort to a combined analytical-experimental approach in order to extract the material behavior from the experimental measurements, with a priori assumptions regarding the constitutive behavior of the material.

* Corresponding author.

0020–7683/99/$ - see front matter
PII: S0020–7683(98)00004–3

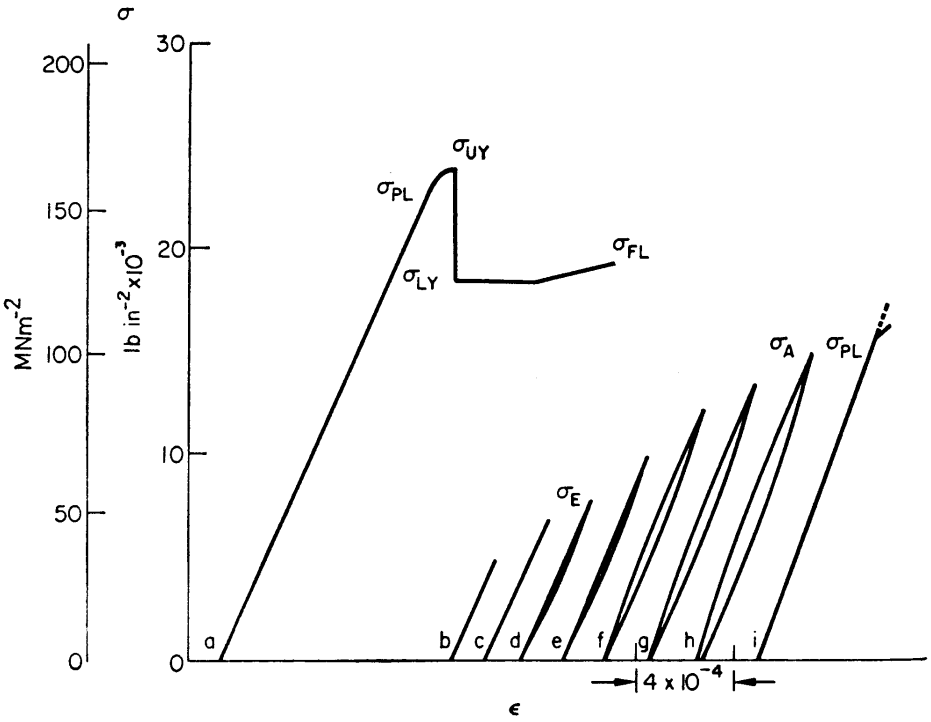

Fig. 1. Nominal stress–strain curve determined by Brown and Ekvall, (1962), indicating evolution of inelastic deformation in α-iron (reproduced with permission).

Of course, such problems of localization are not new; in metallic materials, deformation localization in the form of Lüder's bands occurs at a characteristic angle beyond a critical strain level. The resemblance of the tensile response of polycarbonate to that of metallic materials is indeed quite striking; this is in spite of fundamental dissimilarities that exist at the atomic/molecular and microstructural level, both in terms of the structural long range order and the micromechanisms that govern deformation at the local level. The subject of yield-point phenomenon, Lüder's band formation, and growth has received much attention and is discussed in great detail in the monograph by Hall (1970). In order to set the stage for exploring the similarities, a brief summary is provided here. We begin with the behavior of α-iron taken from the work of Brown and Ekvall (1962). A typical tensile response curve from a strip specimen of α-iron is shown in Fig. 1. The true elastic limit of the material is indicated in the figure as σ_E; this is the stress level above which the stress strain curves begin to show a loop during a loading–unloading cycle. σ_A is the strain level above which a permanent strain is observed upon removing the applied load; this is taken as evidence that plastic flow occurs well below the upper yield point in such materials, σ_{UY}, which is considered to be a nucleation stress for the formation of the first Lüder's band. This stress is usually explained and analyzed in terms of the stress required to breakaway dislocations locked at solute atoms or other pinning sites. The upper yield point cannot be considered as a true material property and experimental measurements of this stress level are subject to large errors due to variations in the microstructure that lead to nucleation of the band at different global stress levels.

The lower yield point, σ_{LY}, is the propagation stress for the continued growth of the Lüder's band and is more easily measured in experiments. Lomer (1952) points out that a close examination of the deformation, in addition to the load-elongation measurements is essential in order to determine the behavior of the material. In particular, the drop in the stress and the plateau region cannot be interpreted as material properties since the deformation in this region is inhomogeneous; thus the formation of the Lüder's band is associated with a load maximum, but not necessarily a stress maximum. He made careful measurements of the angle at which the bands appear and concluded that they range from about 48 to 65° to the loading axis. Once a Lüder's band is nucleated, as the applied global extension of the specimen continues, the band spreads until the entire specimen is strained to the level of the Lüder's strain ε_L. Analytical prediction of the band angle hinges on two crucial observations: first, the material undergoing large inelastic deformation in the band is incompressible; second, the constraint provided by the surrounding material where the deformation is small compared to the Lüder's strain, ε_L, limits the strain in the band parallel to the band to be very small. These two observations have been used by a number of investigators in determining the band angle (Hill, 1948; Nadai, 1950; Hetenyi, 1952; Thomas, 1961). While the Hill analysis arises simply from kinematic considerations, Thomas (1961) used the deformation plane-stress theory of plasticity to analyze a rigid-plastic material completely and determined the band angle by imposing equilibrium equations, incompressibility, yield condition, and the jump conditions at the band boundary. The predicted angle of the Lüder's band is 54.74° from the loading direction, which is very close to the experimentally measured angle of around 55°. It is interesting to note that while the crystallographic slip planes that dictate local plastic deformations may vary significantly from grain to grain, the Lüder's band direction is dictated by the continuum considerations as long as the grain size is small; in coarse grained materials, a diffuse shear band forms and may not even be clearly identifiable in some materials (Hall, 1970). An important question that is still unresolved concerns whether the formation of a Lüder's band is a true material instability or a geometrical instability; there is quite a lively debate on this issue and we shall not get into it here other than to point out that the band orientation is clearly determined by the continuum field and not by crystallographic considerations.

All of these observations on the nucleation and growth of the localized deformation bands in α-iron apply to a class of shear yielding polymers as well! In fact, localized deformations under uniaxial tension that occur in phase transforming ceramics such as zirconia and shape memory alloys (Shaw and Kyriakides, 1996) are also very similar to the problem of Lüder's band development in metals. In this paper, we begin with a detailed experimental examination of the macroscopic deformation localization problem by exploring the tensile response of polycarbonate. After establishing the extent of the similarity between the polycarbonate and the metallic materials described above, the tensile response is simulated numerically using a simple continuum plasticity model for the constitutive behavior of the polycarbonate. Implications on the experimental characterization of amorphous materials using the tensile response of polymers are also discussed.

2. Tensile response of polycarbonate

In this paper we shall focus attention on polycarbonate (PC) as a representative member of the class of shear yielding polymers. While time and rate dependence of the material are inherently coupled and important in analyzing the inelastic deformation and localization, we shall consider

here only the short time response in the glassy state and defer consideration of time and rate effects to a later study. In order to motivate a discussion of the constitutive behavior of PC, we begin with a description of a displacement-rate controlled tensile test along with the observations of the corresponding deformation behavior. The sequence of events observed in a tensile test is different depending on the geometry of the specimen; we describe observations on specimens with a rectangular cross-section. In Fig. 2, the load–elongation diagram from a tensile test in a polycarbonate specimen with a rectangular cross-section (25.4 mm $\times$ 6.35 mm) is shown; at several points during the extension of the specimen, a small unloading step was imposed to determine the extent of the inelastic deformation. The global similarity of the tensile response of the polycarbonate in Fig. 2 to the tensile response of α-iron shown in Fig. 1 is obvious; the primary difference appears in that while the α-iron exhibits a sharp drop in the load beyond the peak, the polycarbonate indicates a rather smooth decrease; the rapidity of the load drop beyond the peak, however, depends on the details of the particular test and is influenced significantly by the dimensions of the specimen and the rate of cross-head displacement relative to the rate of appearance of the localized deformation. The uniformity of the deformation over the entire length of the specimen was examined by capturing the deformation using a video camera at moderate magnifications. The variation of the deformation over a portion of the specimen at different stages in the loading process is shown in Fig. 3. In Fig. 2, clearly five regions are distinguishable, while in earlier work (Buisson and Ravi-Chandar, 1990), we had distinguished only four stages in the deformation behavior, ignoring the nonlinear region prior to the peak-load. The deformation is macroscopically homogeneous in Stages I and II; localized deformation appears in Stage III as a macro shear band visible to the naked eye, coincident with the peak load which then becomes a stable neck profile and propagates along the length of the specimen in Stage IV. Finally in Stage V, homogeneous deformation is re-established over the entire length of the specimen. Details of each stage of deformation are described below, along with comparison to the Lüder's band development in metals.

2.1. Stage I

In Stage 1 of the deformation, a linear behavior is observed and the deformation is macroscopically homogeneous; the deformation is also elastic resulting in instantaneous recovery of the deformation upon unloading; the stress level beyond which load–unload behavior indicates loops is labeled σ_E in Fig. 2, just as in the case of the α-iron. Clearly this value is dependent on the temperature and strain rate; we do not attempt to characterize this material property and its temperature and rate dependence in the present paper, although this would be important in developing a complete constitutive characterization of polycarbonate. The measured elastic modulus from this stage is 2.4 GPa, in agreement with the generally quoted value for PC.

2.2. Stage II

Beyond σ_E, the loading–unloading curves indicate a distinct looping behavior; unloading completely results in an unrecoverable strain that is clearly the result of an inelastic deformation mechanism. The inelastic deformation should be due to a molecular level mechanism; many models, phenomenological as well as mechanistic, have been proposed to model the inelastic behavior of glassy polymers. Argon (1973) proposed a double-kink mechanism to model the barrier

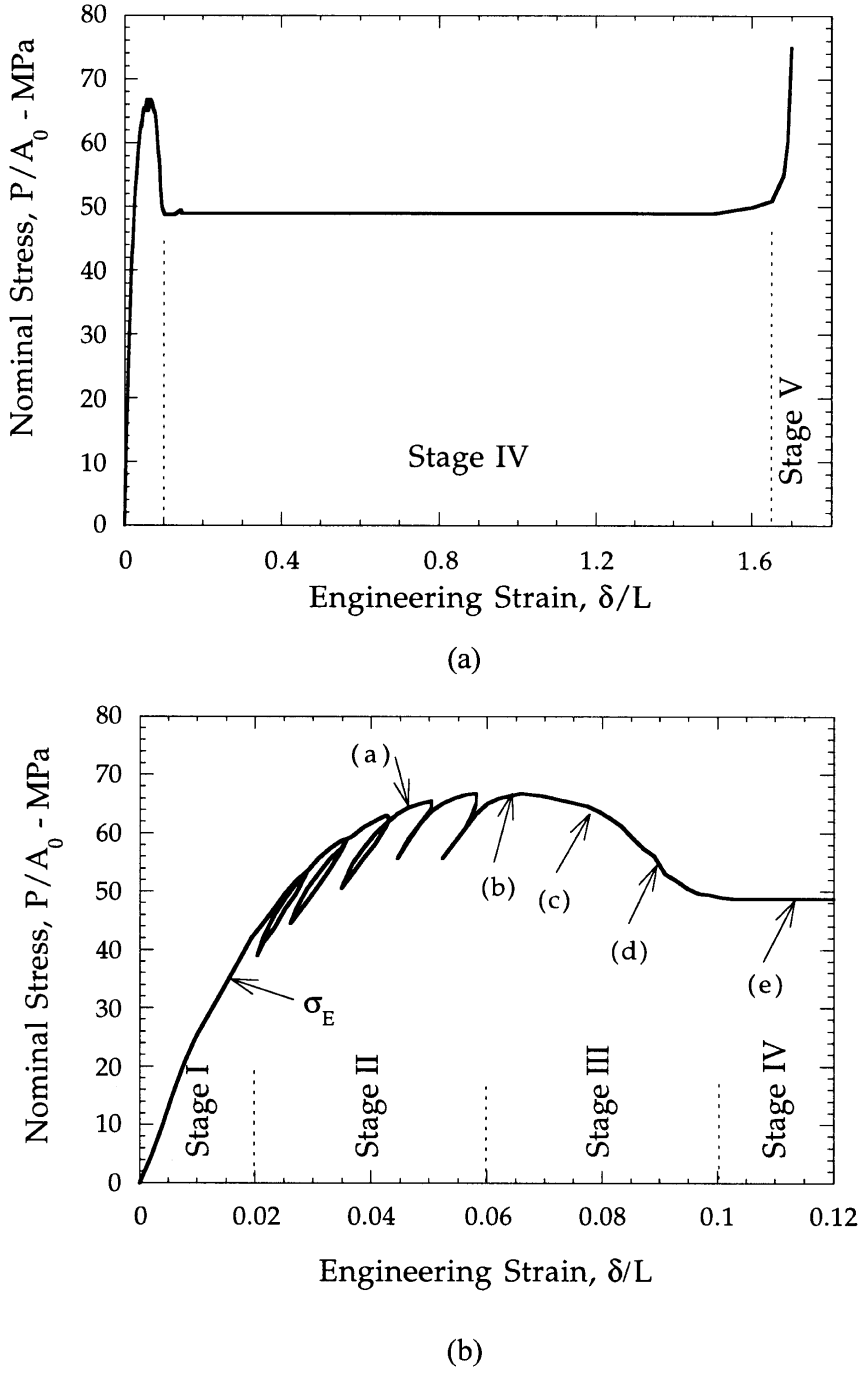

Fig. 2. Nominal stress vs nominal extension of a polycarbonate specimen, indicating the different stages in the deformation. (a) shows the full range and (b) shows an expanded view at small strain levels. Labels (a) through (e) indicate conditions corresponding to the photographs in Fig. 3.

to segmental rotation and estimated the yield stress from elastic modeling of the intermolecular interaction. An activated process rate theory of the Eyring type has been used by a number of investigators to explain inelastic deformation in polymers (see for example, Haward and Thackray, 1968). Nonlinear viscoelastic theories based on stress-induced free-volume changes have also been proposed to explain the inelastic straining (Knauss and Emri, 1987). All of these models are at the molecular scale incorporating activation volumes on the order of a few nm^3; direct evidence of any of these processes cannot be seen, even at the microscale. However, if one observes the specimen in a microscope during Stage II, micro shear bands illustrated in Fig. 3a are seen. A number of observations regarding the micro shear bands are relevant

1. The micro shear bands measuring about 1 μm thick and 100 μm long are observed distributed throughout the specimen, particularly near surface defects. The depth of these bands has not been resolved; thus it is not clear whether these are needle-like or platelet-like structures.
2. Across the shear bands, there exists a large jump in the shear strain; these shear bands are indicative of a true material instability. In this stage, while the local deformation is inhomogeneous, the scale of the inhomogeniety is small and confined by surrounding elastically deforming regions and hence the deformation can be considered to be macroscopically homogeneous.
3. The orientation of these micro shear bands is not controlled by the molecular level inhomogenieties that act as triggers for the micro shear bands. Since the material is amorphous, there is no microstructural texture, such as the slip systems in the grains of polycrystalline materials that would dictate the orientation of the band. The orientation of the micro shear bands appears to be governed by the macroscopic stress state! Bowden and Raha (1970) observed these bands in a plane-strain compression configuration and found the band to be at approximately 45° to the loading direction, while the bands in Fig. 3a, obtained in thin specimens under a nearly plane-stress condition are at an angle of 54° to the loading direction; as indicated earlier, this is precisely the orientation of the Lüder's bands.
4. As the load increases, the density of the micro shear bands increases resulting in a reduction in the overall stiffness of the specimen. This reduction in the stiffness leads eventually to the limit load type behavior of the specimen, with a macroscopic localization of the end of Stage II.
5. The micro shear bands do not disappear with time. Figure 3a was taken from a specimen that was loaded close to the peak-load and then unloaded and left to recover for a period of two months under ambient conditions. Thus the micro shear bands are permanent microstructural rearrangements that require further investigation.

Some investigators refer to this nonlinear region in Stage II as the viscoelastic region since upon unloading, the residual deformation is recovered with time; however, close observations indicate while there is global strain recovery, there is not a microstructural recovery. The micro shear bands remain stable and the global strain recovery is simply due to the relaxation in the surrounding elastic regions with the micro shear bands remaining unchanged.

2.3. Stage III

Corresponding to the peak in the load, which marks the beginning of Stage III, a single macro shear band forms across the specimen cross-section; this is actually a coalescence of many of the

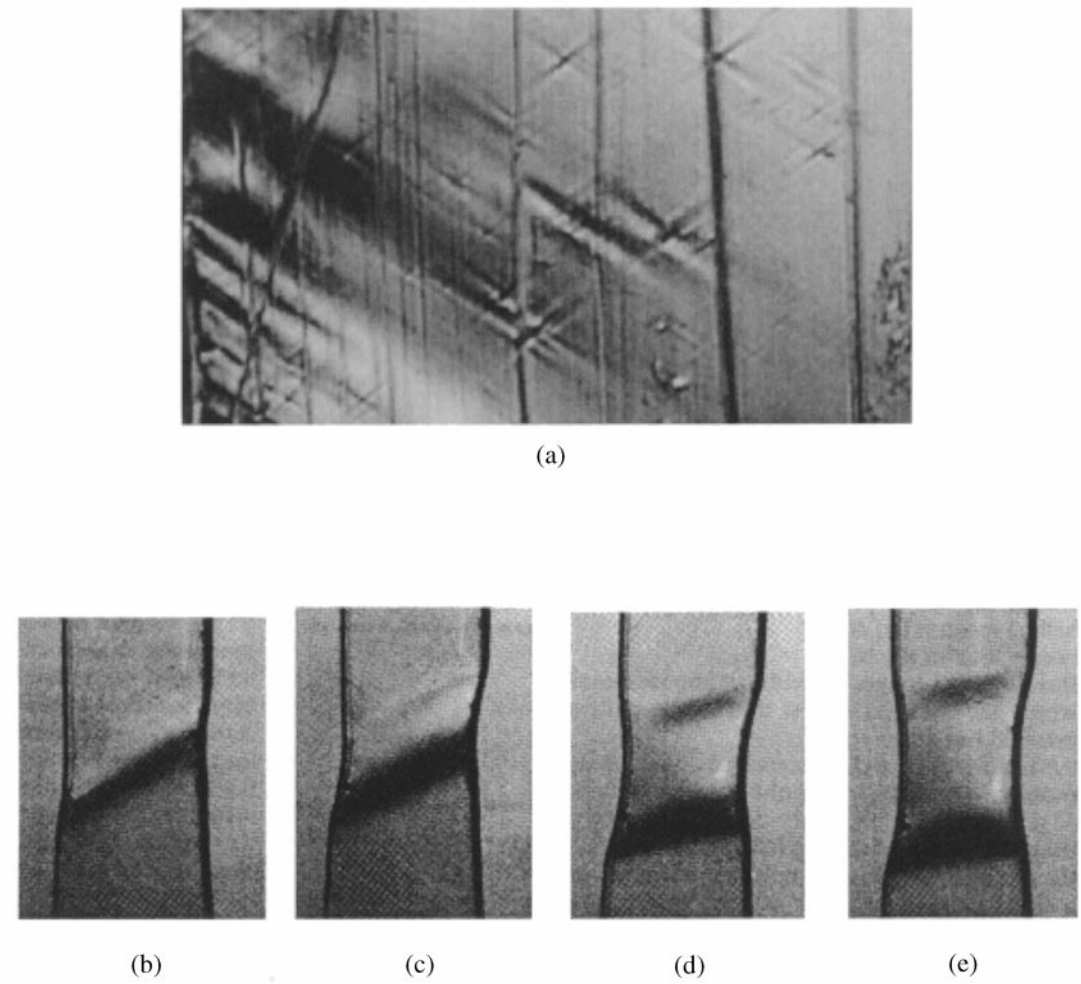

Fig. 3. Micrograph of the polycarbonate specimen taken during Stage II of the deformation is shown in (a); (b)–(d) correspond to Stage III. The formation of the macroscopic shear band across the specimen width, corresponding to the peak-load is seen in (b). In (c) and (d) the future development of the band during the decreasing part of the load–elongation curve is shown. The steady-state neck profile that propagates the length of the specimen is developed as the load–elongation curve plateaus out in Stage IV and is shown in (e).

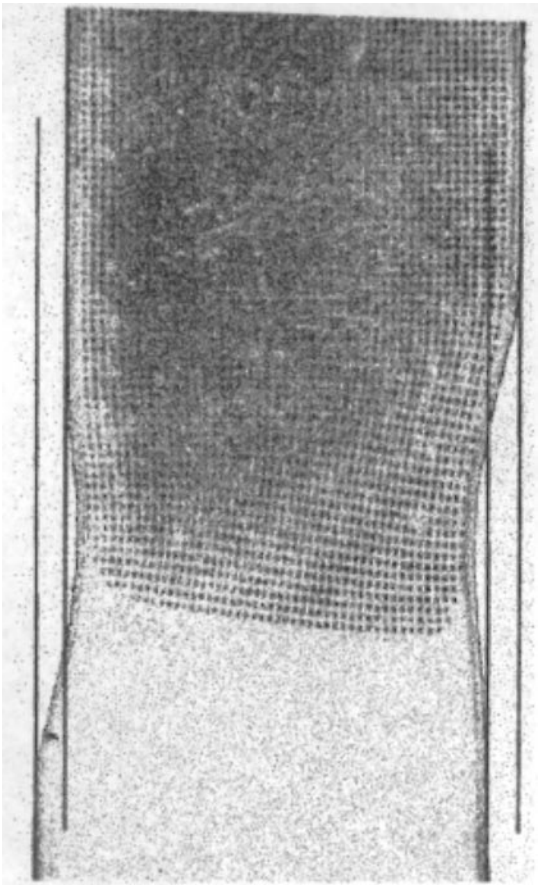

Fig. 4. Photograph of a specimen loaded just beyond the peak load and then unloaded and removed from the groups illustrates the offset generated by the shear band development. In the stiff grips of the loading device, aligning the top and bottom parts of the specimen introduces a bending moment near the band that plays a role in the further evolution of the band. The dots on the specimen were deposited in an effort to evaluate the detailed strain variations within the shear band.

micro shear bands across the entire specimen cross-section; Bowden and Raha (1970) observed a similar coalescence in the plane strain compression test. Beyond this point, the stress and deformation fields are macroscopically inhomogeneous (as we will shown later, even after complete drawing of the neck through the length of the specimen in Stage V) and the load–elongation curve cannot be interpreted as the constitutive behavior of the material. This macroscopic band across the specimen is identical to the fully formed Lüder's bands in polycrystalline materials; the orientation of the band is dictated simply by the macroscopic stress-state, going from about 54° with respect to the loading direction in plane-stress to 45° in plane-strain. One major difference between Lüder's bands in polycrystalline materials and polymers is the fact that the jump in the logarithmic strain (Lüder's strain, ε_L) across the band is only about 3% in most metals and alloys, while it is about 50% in polycarbonate; this large difference in the Lüder's strain influences the propagation of the band across the specimen with continued elongation of the specimen. While Lüder's bands in polycrystalline materials propagate with the same angle as at initiation, the bands in polymers straighten out into a profile that is commonly referred to as a neck. This has, in some instances, led to a confusion of equating this phenomenon with necking which appears in polycrystalline materials at a much later stage in the deformation than the formation of the Lüder's band. Figure 4 shows a close-up view of a specimen that was loaded just past the peak-load to induce the Lüder's band and unloaded; the lateral offset between the two sides of the band is clearly observable in this figure. When the specimen is in a stiff loading machine, this offset imposes a local bending moment across the band which influences its further development; in particular the angle of the band will change from its initial value of about 54° and eventually develop into the necked profile characteristic of these polymers. We note that Mote et al. (1961) investigated the formation and growth of Lüder's bands in a Ag-33 at.% Al alloy single crystal which exhibits a Lüder's stain of 135% and found that the Lüder's bands in this material straightens out into a necked profile before propagating just as in the case of polycarbonate. Thus we characterize this stage as the region where the initial macro shear band is generated and then deformed into a steady-state necked profile, the process occurring at decreasing global load.

2.4. Stage IV

With continued elongation of the specimen, at a constant applied force level, the necked profile generated at the end of Stage III grows up and down along the length of the specimen, entraining new material into the neck. For continued growth of the neck, a necessary condition is that the material must become stiffer at the end of Lüder's strain jump; otherwise, continued straining can occur only in the band and not outside. In the case of polycrystalline materials, this stiffening or increase in resistance to further straining in the band is provided by grain boundaries, while in polymers, it is caused by the generation of molecular orientation at large stretches. Whereas in polycrystalline materials the Lüder's strain can only be considered as a jump strain over a very short length, in polymers, since the Lüder's strain jump is spread out over a significant length, detailed measurements of the stress–strain evolution over the neck is possible and has been attempted experimentally (Buisson and Ravi-Chandar, 1990) as summarised in the next section. The growth of a steady-state necked profile in an axisymmetric geometry has been examined analytically by (Hutchinson and Neale, 1983) using a J_2 plasticity theory. Tugcu and Neale (1987), and Fager and Bassani (1986) examined the plane-strain neck growth problem numerically, again

using a J_2 plasticity theory. All of these investigators used a monotonic stress–strain characterization in modeling the material behavior without intrinsic strain softening; however, the primary interest was in the growth of the neck, with little attention paid to the formation of the Lüder's band.

2.5. Stage V

After the neck propagates along the entire length of the specimen, the fully orientated material in the neck exhibits a large stiffness as the covalent bonds of the polymer chain are now stretched; subsequent incremental deformations are small and elastic. The deformation is also homogeneous over the entire length of the specimen but the stress field may not be homogeneous; birefringence studies of Buisson and Ravi-Chandar (1990) indicate a significant variation in the stress state across the fully stretched cross-section. This region corresponds to the strain hardening region in polycrystalline materials. However, the fully stretched material is elastic and anisotropic as a result of the generation of preferred molecular orientation; the uniaxial loading results in a state of transverse isotropy in the specimen.

From the above description of the tensile response of polycarbonate, two conclusions are apparent

1. The tensile response of polycarbonate is only quantitatively different from that of α-iron and other materials exhibiting the yield point phenomenon. The deformation localization, its stabilization and growth along the specimen in PC are akin to Lüder's band nucleation and growth in metallic materials. What is usually referred to as the 'necking' problem is really the Lüder's band problem for polymers.
2. The tensile response of the rectangular specimen in Stages I and II is readily interpreted as the constitutive behavior of the material in terms of the true-stress vs logarithmic strain. However, the stress fields in Stages III to V are macroscopically inhomogeneous and the tensile response cannot be converted directly into the constitutive behavior of the material, without a detailed experimental analysis of the inhomogeneous deformation and stress fields of the tensile specimen or using an iterative numerical–experimental approach with an assumed constitutive description of the material where numerical results are matched with experimental observations to extract constitutive parameters.

While the variation of the nominal stress with elongation for a bar of circular cross-section appears to be similar to that of the rectangular bar, the circular cylindrical specimen does not always exhibit a distinct macroscopic shear banding at the peak load; instead, the bar deforms directly into a symmetric necked profile. There is a corresponding load drop and once again, the neck grows along the length of the specimen at constant load. Attempts have also been made to measure diametral contraction in the specimen (G'Sell and Gopez, 1985); an hour-glass shaped specimen was pulled in uniaxial tension, with a gauge to measure the diametral contraction along with axial stretching. The tensile response of such specimens is also similar to that described above. We will explore both of these configurations in this paper using numerical simulations.

Clearly, the tensile response of the polycarbonate described here falls into the category of problems described as propagating instabilities by Kyriakides (1994). Thus the peak stress corresponds to the nucleation stress for the localization, which clearly depends on the material and

the geometry of the localization and the constant stress during growth of the neck is the propagation stress. While the nucleation stress can be influenced significantly by defects, the propagation stress remains a predictable quantity, given the constitutive behavior.

3. Constitutive behavior of polycarbonate

From the description provided above, it is apparent that the tensile response cannot be used directly to determine the constitutive behavior of the material. Three options are available now for the characterization of the constitutive behavior. First, an experimental procedure could be used to track the inhomogeneous deformation of the material using experimental techniques that measure field quantities such as displacements or strains and stresses; Buisson and Ravi-Chandar (1990) have used this approach, by combining a grid method of strain measurement and photoelastic method of stress measurement, to examine the evolution of the stress and strain state of a material point as it deforms through a neck; we will summarize this work briefly to motivate our choice of the constitutive behavior. The second approach is to perform experiments in configurations where a homogeneous deformation can be maintained in the inelastic regime; this is a much more difficult task, but we have identified two configurations, one of pure shear with a small superposed pressure and the other one of hydrostatic pressure with a small superposed shear and these will be described in a future contribution. The third approach is to assume a form of the constitutive behavior and attempt to reproduce experimental observations through simulations. The assumed form of the constitutive behavior may be motivated based on micromechanisms of deformation as in the models of Argon (1973) and Boyce et al. (1988), or justified phenomenologically as in the models of Haward and Thackray (1968) and Knauss and Emri (1987). This approach is inherently nonunique primarily from the possibility that more than one constitutive description may be capable of exhibiting the experimentally observed response of the specimen and one may not always have a criterion for discriminating between the different constitutive descriptions.

One major feature in the constitutive characterization of polymers is the issue of strain softening; it is usually assumed that the true-stress exhibits a peak beyond which the true-stress versus strain exhibits a negative slope. Such intrinsic softening behavior of the material is then explicitly introduced into the constitutive description of the material (see for example, Boyce et al., 1988). The evidence for such true-stress softening behavior cannot be from the load drop observed in the tensile response because this load drop is associated with a geometrical instability that triggers inhomogeneous deformation in the tensile specimen. Brown and Ward (1968) put forward the most compelling case for intrinsic softening of the material, through experiments in shear and compression where they observed a load drop. Haward (1973) indicated that the load drop observed in a compression or shear test under isothermal conditions could be taken as evidence of a genuine strain softening behavior of the material. However, only if the deformation is homogeneous in these specimen configurations could the applied loads be reinterpreted in terms of the true-stress; in both the shear and compression configurations, the stress state is not uniform. As demonstrated by Bowden and Raha (1973), beyond the observed load-drop in the compression test, the specimen has a very high density of micro shear bands which introduces an additional mechanism for the deformation of the material and the stress field is far from homogeneous to be

obtained from the global load measurement alone. In the case of so-called simple shear specimen, the presence of the traction free ends introduces a stress singularity at the four corners as well as significant inhomogenieties in the stress field. As observed in G'Sell's (1983) experiments with the rail-shear specimens, the corners of the specimen experience significant stress concentration; Wu and van der Giessen (1994, 1995) analyzed G'Sell's experiment using the strain-softening constitutive model of Boyce et al. (1988), and showed that the stress field in the rail-shear specimen is very inhomogeneous. Thus interpretation of the globally measured load in terms of the true shear stress is questionable. A corollary of this finding is that a measured global load drop in any experimental configuration may not be indicative of intrinsic material softening unless homogeniety of deformation and stress fields is established over the entire specimen or local field measurements are made to demonstrate intrinsic softening; to return to Lomer's (1952) observation, global measurements are inadequate and one must follow the details of the deformation locally.

In Stage IV of the deformation behavior of a tensile specimen of rectangular cross section, part of the specimen is in a fully drawn configuration while the remainder of the specimen has not been inelastically deformed at all; this is shown schematically in Fig. 5. During the steady-state neck growth, the upward movement of the necked profile can be viewed as the material point indicated as A moving down through the Lüder's strain as it arrives at the location B relative to the neck. In the process of the neck propagation or cold drawing, the material point is deformed from the pre Lüder's strain stage (Stage II) to the fully drawn state as these points are processed by the

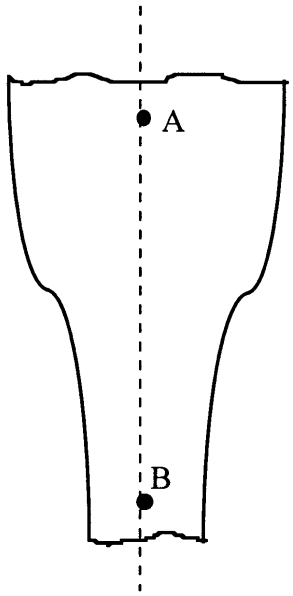

Fig. 5. A schematic representation of the necked profile that propagates in the specimen. From measurements of the deformation of a regular grid pattern on the specimen surface, Buisson and Ravi-Chandar, (1990) measured the strain variation from point A to B, as displayed in Fig. 6. They also measured the birefringence variation from A to B and related it to the stress variation. Correlating the two measurements, a true-stress vs logarithmic strain variation was determined as shown in Fig. 7.

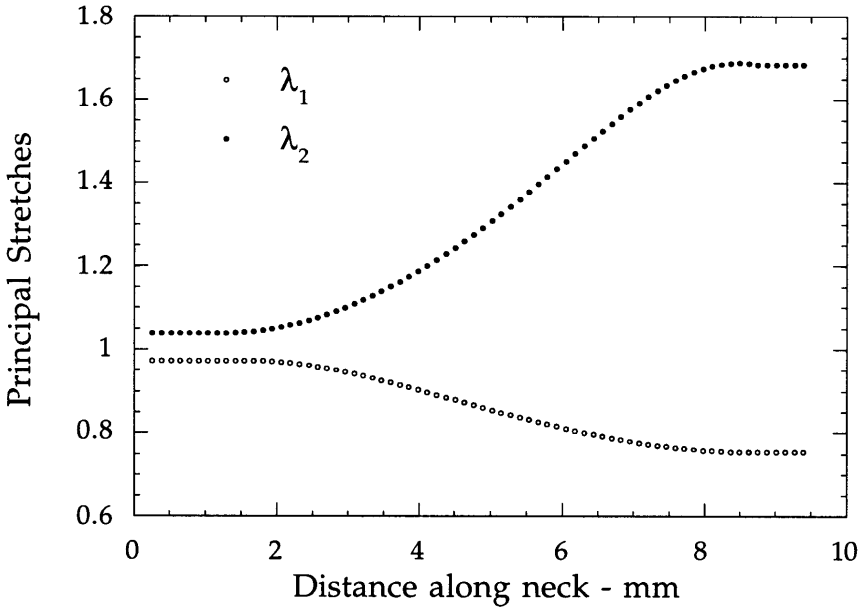

Fig. 6. Variation of the longitudinal (λ_2) and lateral (λ_1) stretches along the center line of the necked profile (from A to B in Fig. 5) from the results of Buisson and Ravi-Chandar, (1990).

growing neck in a stable loading path. Buisson and Ravi-Chandar (1990) examined the experimental characterization of the large deformation constitutive behavior of polycarbonate by performing detailed measurements of the evolution of the inhomogeneous deformation of the material points that are drawn through the neck. A fine grid was deposited in the undeformed specimen and was photographed before loading and again during steady-state neck growth; these measurements enable the complete determination of the strain evolution along the center line of the growing neck from the point A to the point B; this strain profile is shown in Fig. 6, in terms of the principal stretches, λ_2 along the direction of loading and λ_1 normal to the loading direction. The average true stress at points A and B is easily calculated from measurements of the load and cross-sectional areas at these locations. In an effort to determine the stress evolution between these two points, Buisson and Ravi-Chandar (1990) used a technique based on birefringence measurements. Decomposing the birefringence into a form birefringence caused by molecular orientation and additional stress-induced birefringence caused by the applied loading, the true stress variation along the line from A to B was determined. By a pointwise correlation of the measured stress and strain along the neck, the stress–strain path followed by a material point during neck propagation was obtained as shown in Fig. 7. This experimental result suggests a monotonic variation of the true-stress strain relationship without an intrinsic softening in the material behavior.

Motivated by the experimental result described above, the constitutive behavior for polycarbonate is assumed to be trilinear. Thus the true-stress vs logarithmic strain variation under uniaxial tension is postulated to be as follows:

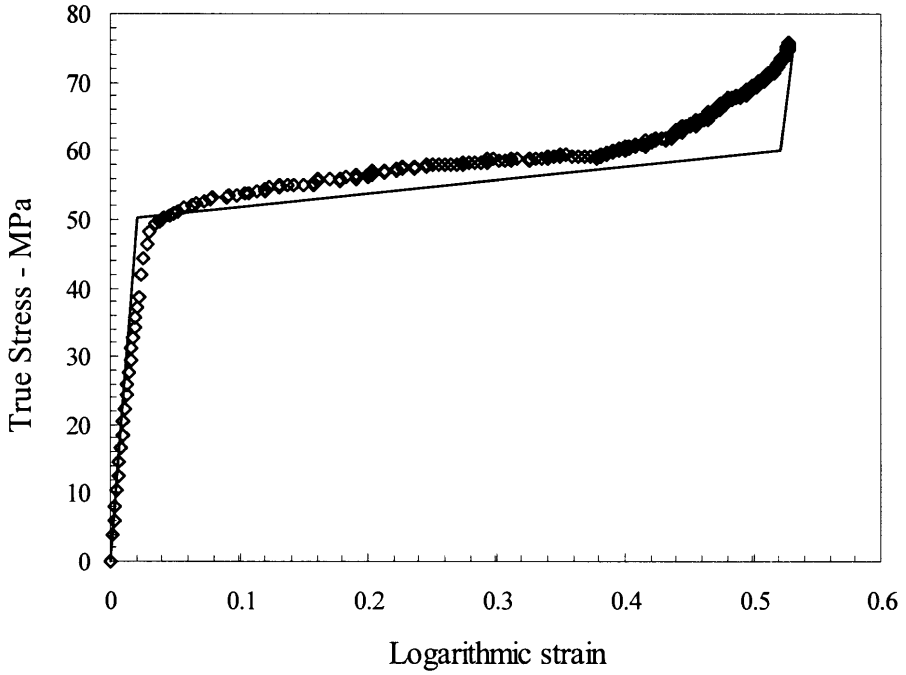

Fig. 7. Variation of the true stress in the direction of extension with the logarithmic strain from the results of Buisson and Ravi-Chandar, (1990); also shown in the figure by the solid line is the trilinear stress–strain behavior that is used in the present paper as an approximation to the measured stress–strain curve.

$$\sigma = \begin{cases} E\varepsilon & \varepsilon \leqslant \varepsilon_0 \\ E\varepsilon_0 + E_t(\varepsilon - \varepsilon_0) & \text{for } \varepsilon_0 \leqslant \varepsilon \leqslant \varepsilon_h \\ E\varepsilon_0 + E_t(\varepsilon_h - \varepsilon_0) + E(\varepsilon - \varepsilon_h) & \varepsilon \geqslant \varepsilon_h \end{cases}$$

The strain ε_0 corresponds to the yield strain, beyond which there is a significant loss of stiffness of the material. ε_h corresponds to the strain at which stiffening caused by the generation of molecular orientation begins, and the modulus is restored to its initial value beyond this strain level. $(\varepsilon_h - \varepsilon_0)$ corresponds to the Lüder's strain, ε_L. E is the initial modulus of elasticity; E_t is the tangent modulus when large scale molecular reorientation occurs. While the stiffness in the fully oriented state can vary considerably in different polymers, here it is taken to be equal to the initial slope. Also, beyond the yield strain, the material is assumed to be incompressible. The generalization of this trilinear stress–strain behavior to multiaxial stress states is accomplished through the standard incremental J_2 theory of plasticity, using a von Mises criterion for yield and the Prandtl–Reuss flow equations. In the simulations described below, the following material parameters were used: $E = 2.4$ GPa, $E_t = 20$ MPa, $\varepsilon_0 = 0.021$ and $\varepsilon_h = 0.521$. The assumed form of the stress-strain curve is shown in Fig. 7 along with the experimentally indicated variation. Note that E_t has been taken to be positive and intrinsic material softening is not introduced in the material model. The inelastic behavior is known to be significantly influenced by pressure, but this dependence is not included in the present model, deferring such considerations to a later investigation.

4. Numerical simulation of the tensile response

We now turn to the numerical simulation of the tensile response of polycarbonate with the constitutive behavior described above. The numerical simulation was performed using the finite element package ABAQUS[1]. The objective of this numerical simulation was simply to demonstrate that the key features of the experimentally observed stages of deformation described earlier as well as the macroscopic tensile response in terms of the load-elongation curve can all be duplicated by the assumed trilinear constitutive behavior, without invoking the idea of intrinsic material softening.

Considering that the tensile response observed experimentally exhibits a localization, the numerical simulation must be performed carefully. Numerous investigators have addressed the issue of deformation localization in numerical simulations (Ortiz et al., 1987; Needleman, 1988; Nemat-Nasser, 1989; Zbib and Jubran, 1992; Shaw and Kyriakides, 1996). Two main strategies have been followed in these simulations: the most common technique for simulation of deformation localization is the four-noded quadrilateral elements that are formed by static condensation of constant strain triangular elements (see Needleman, 1988). Nemat-Nasser (1989) has demonstrated that if reduced integration is used in evaluating the element stiffness matrix of isoparametric quadrilateral elements, one can also simulate deformation localization. Most of the simulations of deformation localization have used plane strain conditions; however, three dimensional simulations have also been performed (see Ortiz et al., 1987; Zbib and Jubran, 1992). While the specimens of rectangular cross-section are perhaps close to a plane stress state, a three-dimensional simulation was performed in order to duplicate the tensile response of the specimen. Our initial simulations were performed with two thin layers of three-dimensional 8-node cube elements, with reduced integration, but similar results were obtained with only one layer in the thickness direction. We note that reduced integration was used only to induce deformation localization with a sharp demarcation; with standard integration, localization of the deformation does appear in the numerical simulation but the bands are more diffuse; perhaps this can be overcome through mesh refinement, but we have not explored this yet. Large strain kinematics were included in the simulation and the incremental loading was determined through the Riks method in order to move in a stable manner through the load drop that arises as a result of the deformation localization.

Needleman (1988) indicated that in rate-independent plasticity models, such as the one used here, deformation localization would be dependent on the mesh refinement, i.e. localization will always initiate over a length scale of one element and that this length scale dependence will disappear as soon as a small rate dependence is introduced. Most of the early investigators were concerned primarily with metallic materials; the material model used involved a rate independent or dependent plasticity theory with thermal softening introduced to incorporate the effect of the heat generation resulting from the plastic work. In these models, once localization appeared, further deformation would be concentrated only in these bands resulting in large gradients of deformation. However, in the material model used in our simulations, the small positive tangent modulus assumed during the development of the Lüder's strain and the generation of molecular

[1] We are grateful to Hibbitt, Karlsson and Sorensen, Inc., for providing the ABAQUS code to the University of Houston under an academic license.

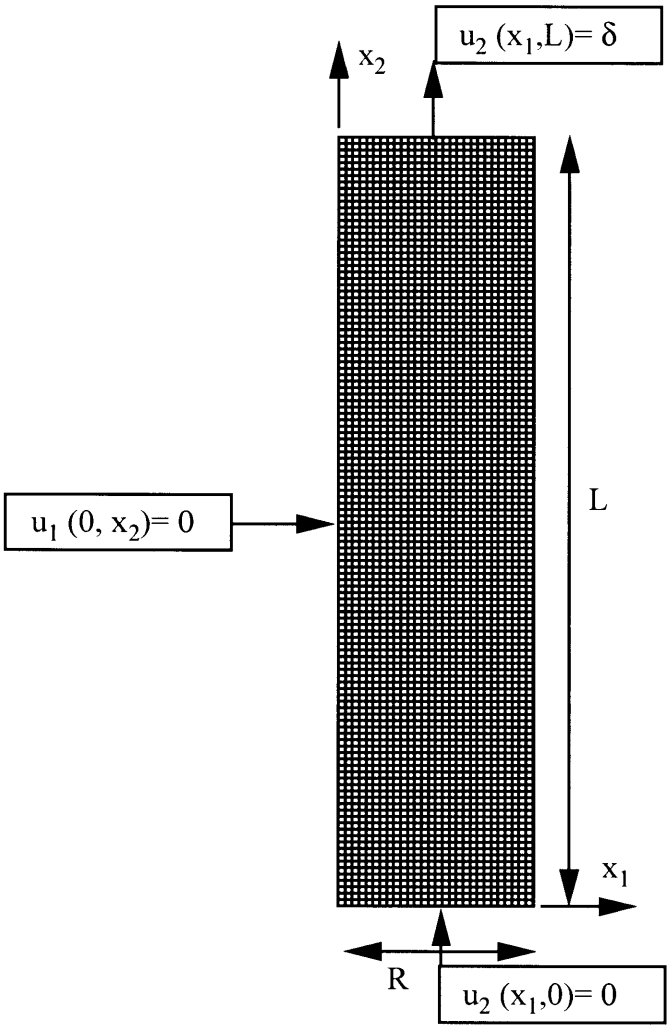

Fig. 8. Sketch of the geometry used in the numerical computation. The depth to width to height ratio was 1:30:120. The prescribed displacement components are shown; all other displacement degrees of freedom were left unconstrained. The bottom layer (not shown in the figure) was constrained to have a zero displacement in the x_3 direction.

orientation that restores the modulus to a high value beyond ε_h makes the numerical stability problems disappear. Still, the initial localization of the shear deformation would be influenced by the element size. Our primary interest was in examining the development of the macroscopic shear band qualitatively; if the macro shear band at the peak-load is to be simulated appropriately, then very small elements are required. A mesh sensitivity study was performed to determine that the variations in the load–elongation curve were not significant as discussed below.

The numerical simulation of a bar of rectangular cross section is discussed first. Due to the symmetry only one eighth of the specimen was modeled; a diagram of the simulated model is shown in Fig. 8, indicating the coordinate system and the displacement constraints. Symmetry

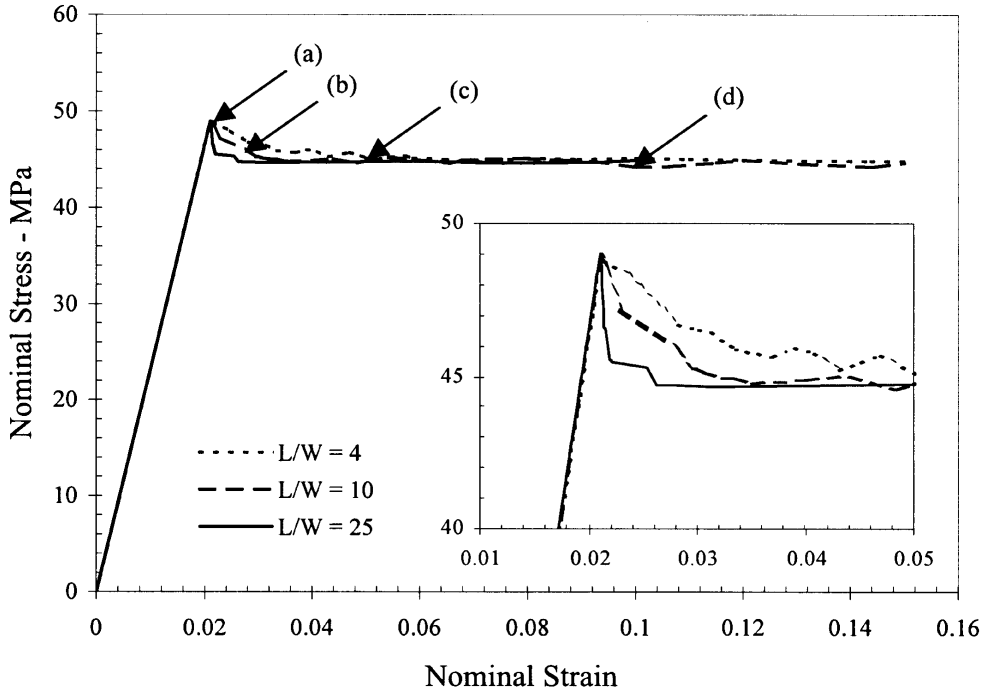

Fig. 9. Numerically simulated tensile response of the rectangular specimen, indicating the engineering stress–strain curve. Note that a load drop appears that corresponds to the initial formation of the localized deformation across the specimen width. Labels (a)–(d) indicate the load and strain levels corresponding to the results displayed in Fig. 11. The effect of the specimen aspect ratio influences the rapidity with which the localization sets in; this is indicated in the inset plot, where the region near the peak load is expanded.

boundary conditions were imposed on the planes $x_1 = 0$, $x_2 = 0$ and $x_3 = 0$; on $x_2 = L$, the applied displacement δ was imposed in the x_2 direction, without constraining the degree of freedom in the x_1 direction. The aspect ratio of the specimen (length, L, to width, w, to thickness, t) was taken to be 4:1:1/30. The mesh was taken to be uniform cubes, with a side equal to the thickness; through many trials on coarse meshes, it was determined that a single layer of elements was sufficient to show the localization behavior. The total number of elements used in the model was 3600 ($1 \times 30 \times 120$ depth $\times$ width $\times$ length). Using a coarser mesh (900 elements) did not influence the results significantly. A small material defect, amounting to a 2% drop in the yield stress, σ_0, was introduced in the corner element at $(0, 0, 0)$ in order to trigger the localization; all other material parameters were maintained constant. The variation of the global load with the extension, normalized to indicate the nominal stress vs engineering strain over the entire specimen length, is shown in Fig. 9. In Fig. 10, contours of constant effective plastic strain are shown at different global strain levels just at the onset of the deformation localization, at strain levels from 2.1025 to 2.105%. In Fig. 11 contours of constant effective plastic strain at strain levels up to 10% are shown. Note that in both these figures, only a portion of the simulated region is shown for clarity. The main result of this numerical simulation is that the trilinear constitutive relation that was assumed is able to reproduce the observed tensile response of polycarbonate, without intrinsic material softening. The exper-

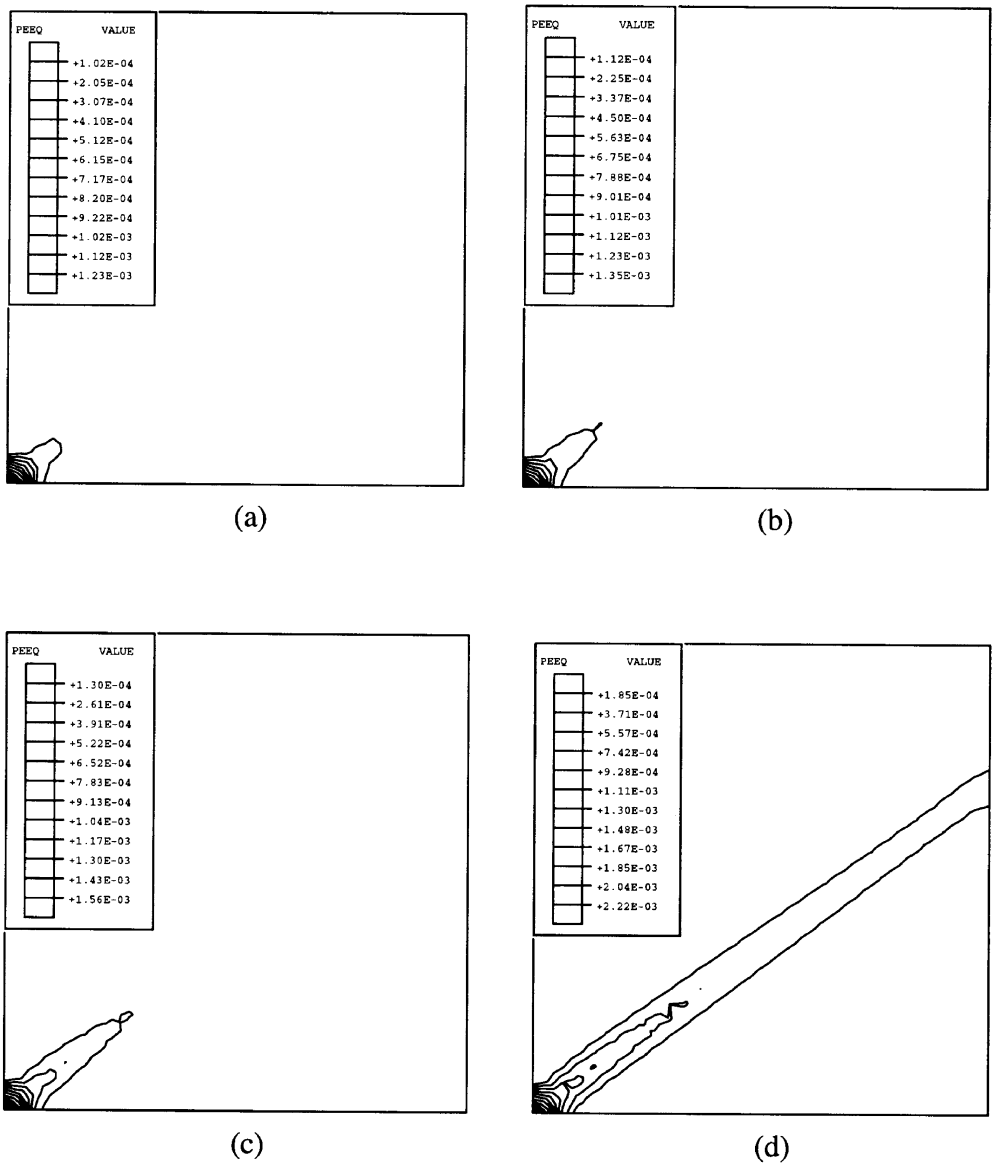

Fig. 10. Initiation of the shear band as indicated by contours of equal effective plastic strain; as the global strain increases by a small amount, the shear band shoots out at an angle of about 35°. Note that while the aspect ratio of the specimen is 4:1, only a portion of the specimen height is shown in these figures. The four figures correspond to the following strain levels: (a) 0.021025, (b) 0.021033, (c) 0.021042, and (d) 0.02105.

imental observations of the tensile response that are reproduced in this numerical simulation are discussed below

1. The global load–elongation curve shown in Fig. 9a resembles the tensile response of the PC.

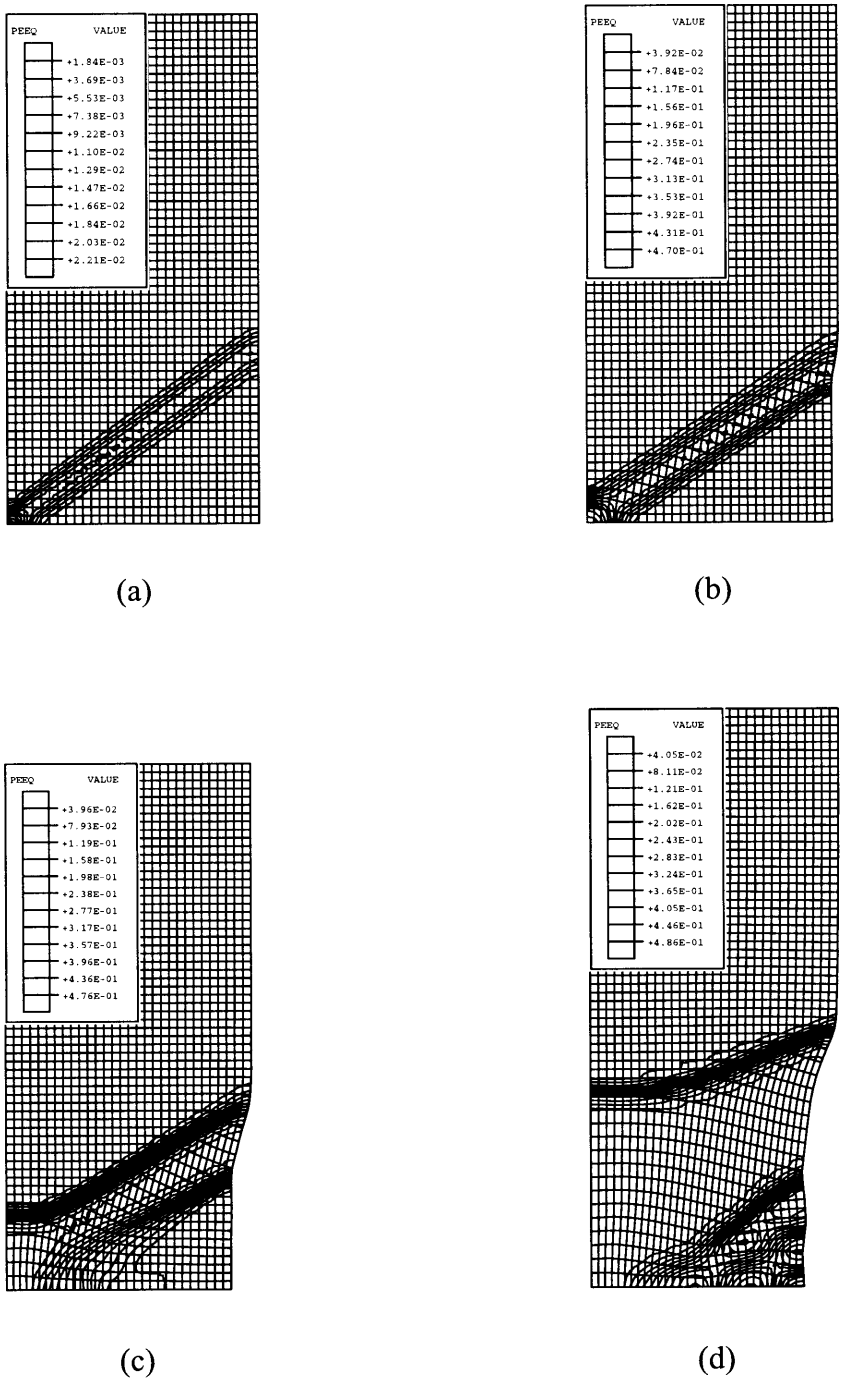

Fig. 11. Growth of the macroshear band in polycarbonate. This figure shows the deformed mesh as well as contours of equal effective plastic strain at different engineering strain levels. The four figures correspond to the following strain levels: (a) 0.0213, (b) 0.03, (c) 0.05, and (d) 0.10.

In particular, the peak-load behavior exhibited by PC during macroscopic shear banding is observed in the simulation as well.

2. The onset of the localization is quite slow; however, this is a structural phenomenon and not related to the constitutive behavior of the material. The load–elongation curves for two other simulations where the L/w ratio of bar was changed to 10 and 25 are also shown in Fig. 9. An expanded plot, focusing on the peak-load region is shown inset in Fig. 9. Clearly, the longer specimen exhibits localization much more rapidly; in fact, in experiments, if a very long bar is used, it is possible to break the specimen at the onset of localization. This is because the release of energy from the remaining part of the specimen (away from the localization) is quite large and equilibrium development of the localization and further propagation are not possible.
3. The magnitude of the load drop in the numerical simulations is about 9%, somewhat smaller than that obtained in the experiments. However, the magnitude of the load drop depends on a number of factors—nonlinearity prior to peak load, rate dependence, thermal softening due to heating—that have been excluded from consideration in the simple trilinear model used in the present simulation. As a simple check, if the modulus in the middle segment E_t is changed from 20 to 10 MPa, the magnitude of the load drop is about 16%. Thus taking into account neglected effects might bring the load-drop in the simulation closer to that observed in experiments.
4. At the peak load, which occurs precisely at the yield strain, ε_0, the deformation localizes along a very narrow band as shown in Figs 10 and 11. This coincidence of the peak load with yield strain is, of course, a result of the trilinearity of the assumed material behavior; if Stage II nonlinear behavior is included in the constitutive description, localization will appear later. With the formation of this Lüder's band, further deformation is concentrated in this region and the global load drops.
5. It is seen that the localization progresses at an angle of about 55° with respect to the loading direction, just as observed in the experiments.
6. As further deformation is applied at the ends of the specimen, large plastic straining occurs in the band, while the regions outside experience very little plastic straining. If the material were perfectly plastic, further deformation will occur only in the band; however, since the polycarbonate is assumed to stiffen up with the realignment of the molecules along the stretching direction, the plastic strain in the band is limited to $(\varepsilon_h - \varepsilon_0)$. At this stage, the modulus of the material is restored to its initial value and further deformation can occur in the band only by increased loading; however, the material adjacent to the band is still capable of large deformations through the Lüder's strain $(\varepsilon_h - \varepsilon_0)$ and hence the band begins to grow along the length of the specimen at nearly constant load. This growth of the band is shown in Fig. 11 where the deformed grid is shown along with the contours of effective plastic strain at four different applied global strain levels. The strain levels corresponding to these are marked on the load–elongation diagram in Fig. 9.
7. The initial Lüder's band angle of 55° to the extension direction is not preserved during the propagation of the band. As seen in Fig. 11, the band straightens out into the characteristic necked profile typically observed in experiments.
8. Continued propagation of the band occurs at a constant force again just as in the experimental observations.
9. Figure 12 shows the contours of constant normal stress in the direction of loading at different

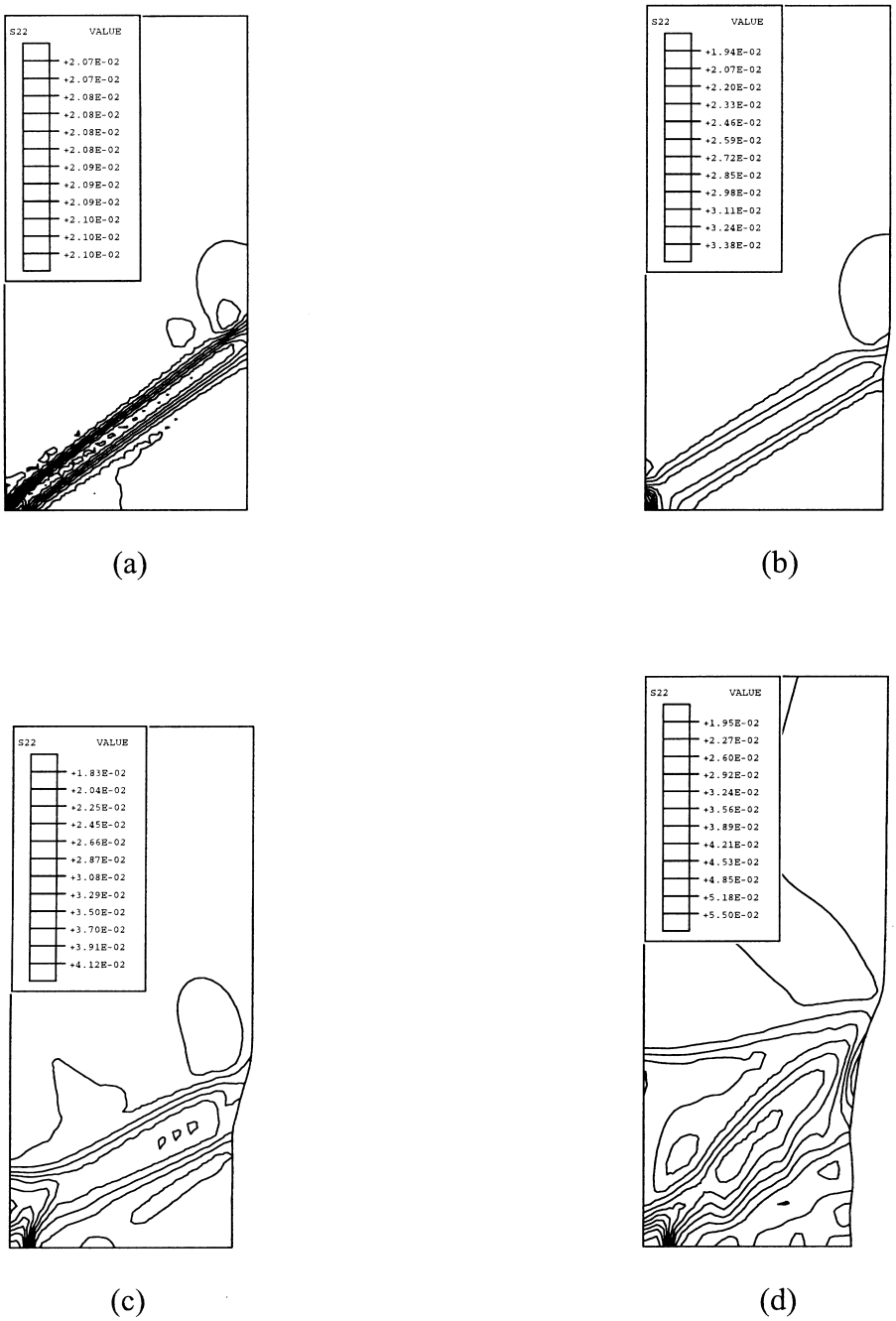

Fig. 12. Contours of the normal stress σ_{22} corresponding to the following strain levels: (a) 0.0213, (b) 0.03, (c) 0.05, and (d) 0.10.

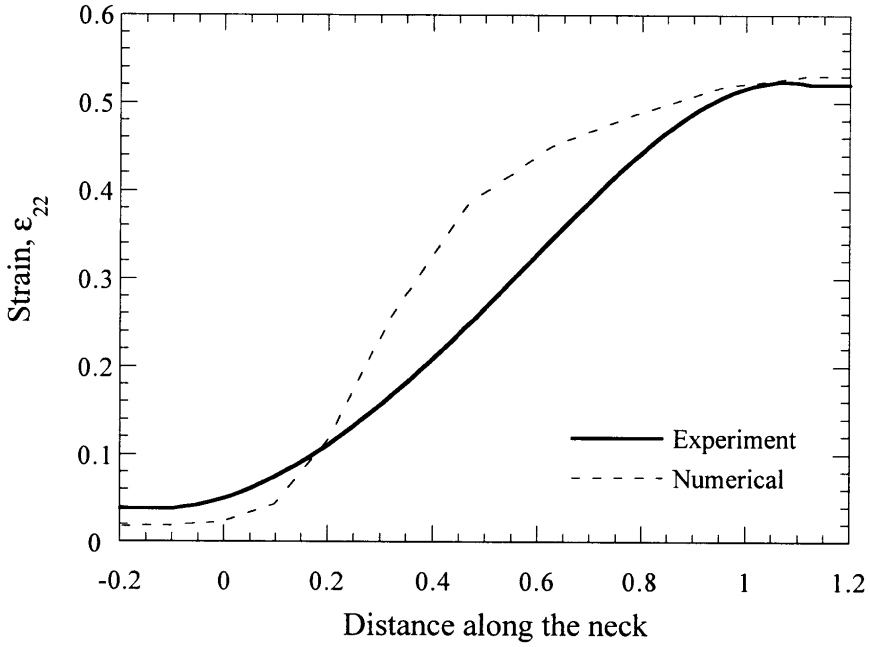

Fig. 13. Comparison of the variation of the longitudinal strain ε_{22}, along the length of the neck.

global strain levels; clearly this stress is not uniform across the cross-section of the specimen, even after the necking deformation has fully encompassed a region; the implication is that the globally measured load-elongation behavior during Stage V cannot be directly related to the stress–strain behavior due to the inhomogeneity in the stress and strain fields.

10. The strain profile along the neck measured experimentally by Buisson and Ravi-Chandar (1990) are compared with the strains determined from the numerical simulation in Fig. 13; while there are quantitative differences in the strains, the evolution of the strain from the unstretched to the stretched region appears to be qualitatively similar; the differences arise primarily from the idealized trilinear constitutive description.
11. The variation of the true-stress component σ_{22} across the specimen width at the top and bottom boundaries ($x_2 = 0$ and $x_2 = L$) is shown in Fig. 14. While the stress is uniform at the top, a large variation is seen along $x_1 = 0$; clearly, the measured global strain and the average stress in the gauge sections are not to be interpreted in terms of the constitutive of the material.

In summary, Stages I, III and IV of the experimentally observed tensile response are reproduced in the simulation as well. Stage II nonlinear behavior, before the peak load, is caused by the micro shear banding and cannot be duplicated in the simulation because of the scale of the discretization and the homogeneity assumed in the elements. The simulation was not performed up to full stretch of the specimen to obtain Stage V response, but this is simply due to computational expense. Thus it appears that the trilinear material behavior does very well in capturing, qualitatively, all the features of the tensile response.

In an effort to circumvent the shear banding instability observed in specimens of rectangular

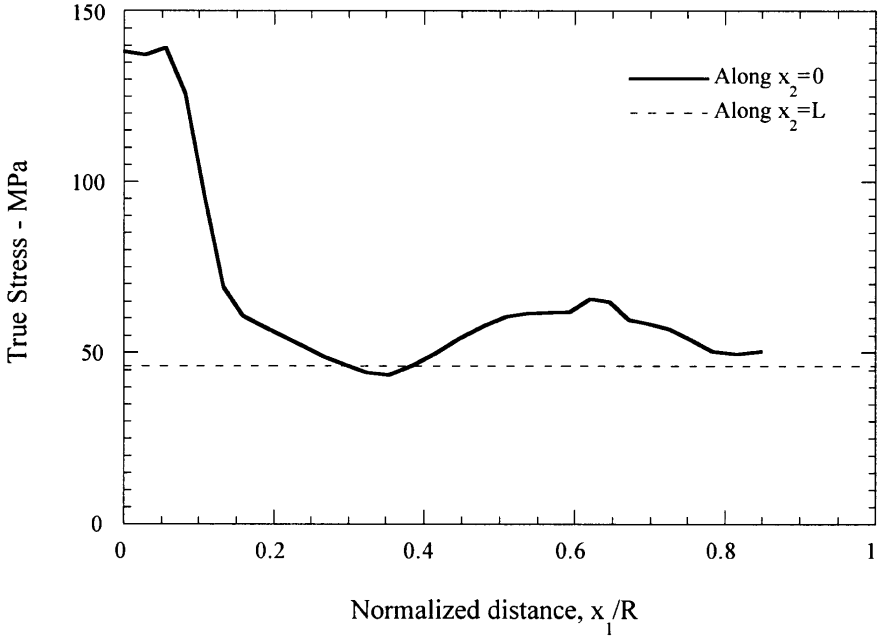

Fig. 14. Comparison of the variation of the x_2 component of the true normal stress across the specimen at $x_2 = 0$ and $x_2 = L$.

cross-section, uniaxial tensile experiments are also typically performed on circular cylindrical and hour-glass shaped specimens (see for instance G'Sell and Gopez, 1985; Boyce et al., 1994); typically, the shear banding localization behavior described above with respect to the rectangular cylinder is not observed in these geometrical configurations. In the circular cross sections, the radial symmetry required of the deformation prevents the appearance of an asymmetric neck. The deformation progresses from a homogeneous extension initially into a necked profile similar to that which appears at much later stages in the rectangular specimens. This, however, is not always true; we have observed the formation and growth of macroscopic shear bands in circular cylindrical specimens, perhaps due to a small ellipticity in the cross section of the machined specimens or misalignment in the loading grips resulting in a small asymmetry. In these experiments, the applied load and extension measurements are usually supplemented by measurements of the specimen diameter using an extensometer; this enables the interpretation of the load in terms of an average true-stress.

Numerical simulations of the circular cylindrical and hour-glass specimens were performed using the same trilinear stress strain curve described above. In order to allow for the possibility of non-axisymmetric deformations the circular cylindrical specimen was modeled completely, without using the axisymmetry conditions. A small material defect was introduced in one element, to provoke asymmetry; however, the resulting localized deformation quickly developed into the axisymmetric mode, perhaps due to the coarse nature of the mesh; thus all simulations of the circular cylindrical and hour-glass shaped specimens were performed using axisymmetric finite elements in the configurations shown in Fig. 15. A geometric defect was introduced in the circular

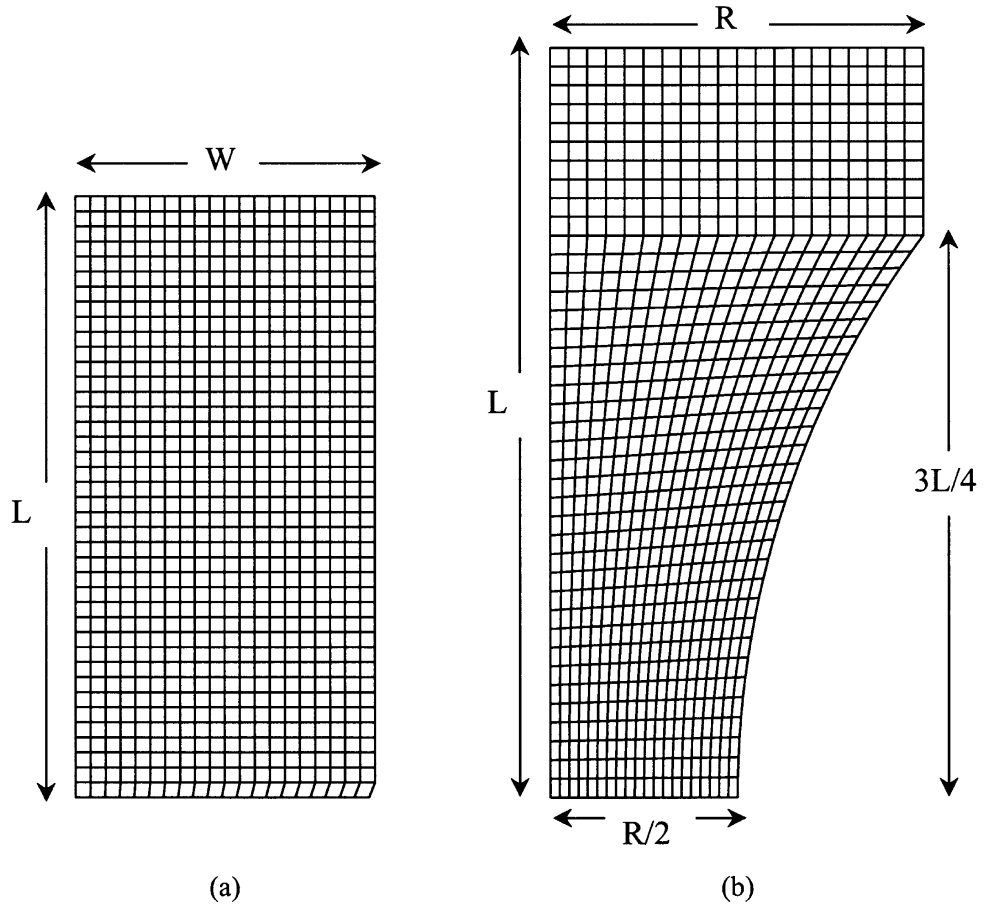

Fig. 15. Details of the axisymmetric finite element mesh used in the simulation of the tensile response of the circular cylindrical and hour-glass shaped specimens. A 2% geometric defect was introduced in the bottom right hand corner element.

cylindrical specimen at the bottom line of elements element to trigger the localization; no trigger was necessary for the hour-glass shaped specimen due to the inhomogeneous nature of the stress field in this specimen configuration. Once again, symmetry boundary conditions were imposed on the planes $x_1 = 0$, and $x_2 = 0$; on $x_2 = L$, the applied displacement δ was imposed in the x_2 direction, without constraining the degree of freedom in the x_1 direction. Using reduced integration in evaluating the stiffness matrix still presents the ability to exhibit sharp deformation localization patterns in the axisymmetric problem. The observations from the numerical simulations on these two configurations are discussed below

1. The tensile response of the circular cylindrical and hour-glass specimens are shown in Fig. 16. The total elongation normalized by the total length of the cylinders is plotted in the abscissa. The load, obtained by summation of the nodal forces at the top line of nodes where the displacements were prescribed simulating the experimental displacement-controlled loading

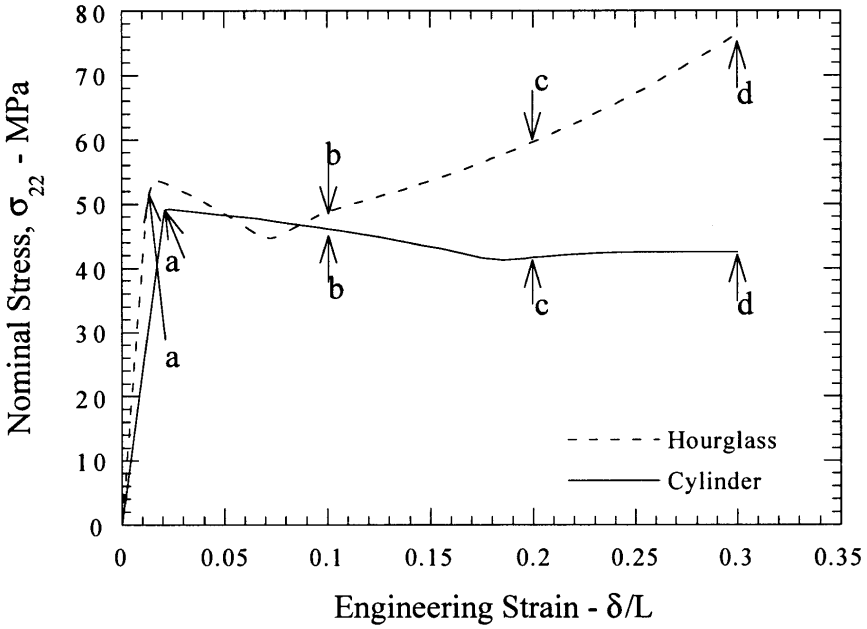

Fig. 16. Tensile response of the circular cylindrical and hour-glass shaped specimens; for the hour-glass shaped specimen, the force is normalized by the initial waist area. Labels (a)–(d) indicate the strain levels at which details of the stress and strain field are displayed in the following figures.

scheme and normalized by the initial cross-sectional area, is plotted in the ordinate; for the hour-glass shaped specimen, the initial waist area is used. The global tensile response is similar to that observed in experiments (Boyce et al., 1994); a peak-load is observed in the response corresponding to a necking localization of the deformation.

2. The deformed profiles corresponding to the labels (a) through (d) in Fig. 16 for the circular cylindrical and hour-glass shaped specimens are shown in Figs 17 and 18 respectively; contours of effective plastic strain are also plotted in this figure. Clearly, in the circular cylindrical specimen, there is an initial tendency for the growth of localized deformation at 45°, but this quickly develops into a necked profile at larger strains. The inhomogeneous stress field in the hour-glass shaped specimen forces a neck to develop from the minimum cross-sectional region.
3. For the circular cylinder, growth of the neck along the length of the specimen occurs initially at decreasing load and after a steady-state profile is attained the neck grows at constant nominal stress; this observation is similar to the results of Tugcu and Neale (1987). On the other hand, for the hour-glass shaped specimen, while there is an initial drop in the nominal stress due to the localization, the tapered profile of the specimen does not allow for a steady-state neck profile to develop; beyond the initial load drop, the neck grows along the specimen length at increasing nominal stress.
4. The tensile response of the hour-glass shaped specimen was determined experimentally by Boyce et al. (1994) who also performed a numerical simulation using a constitutive model developed by Boyce et al. (1988) and Arruda and Boyce (1993); intrinsic softening of the material is

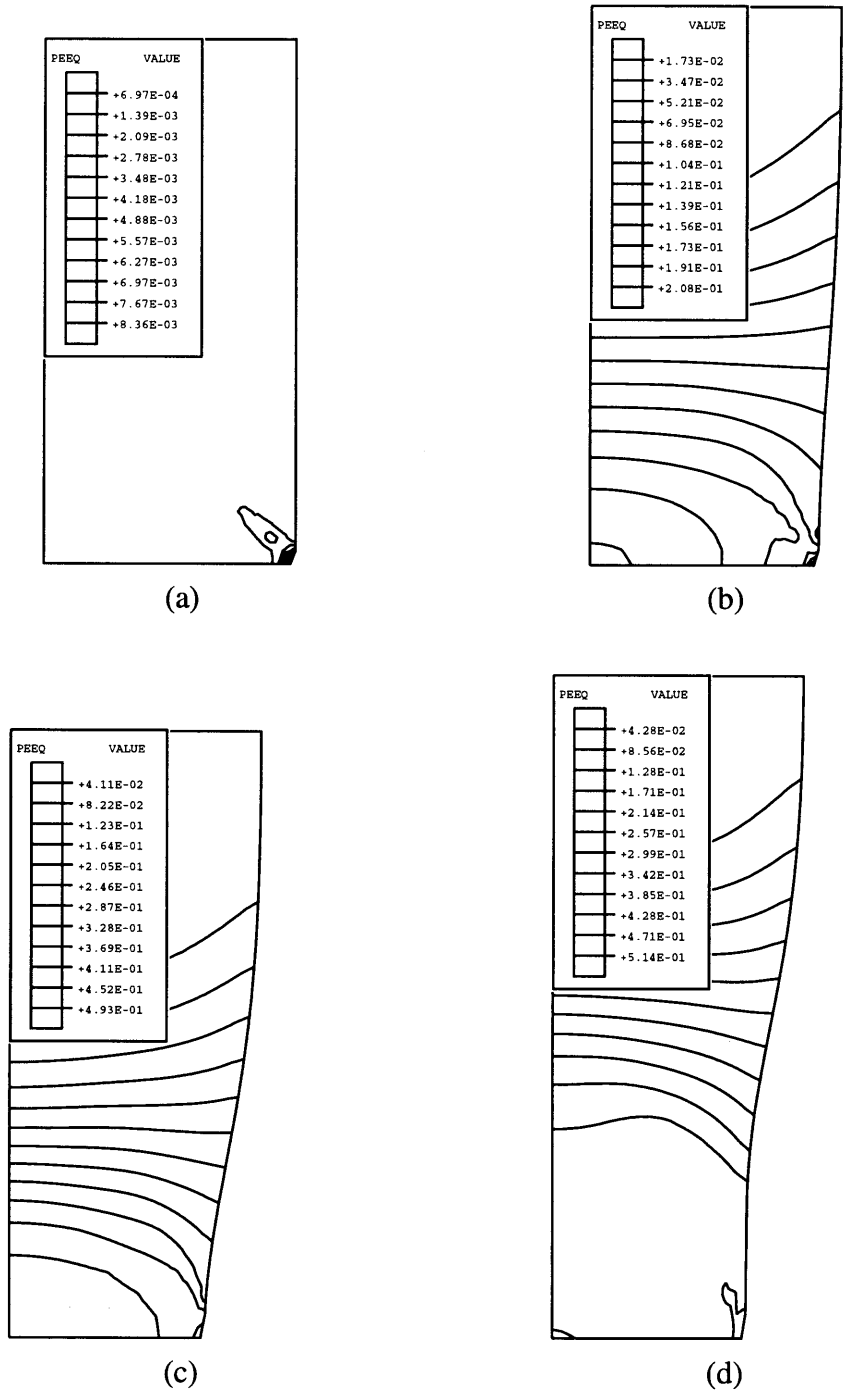

Fig. 17. The figures shown the contours of constant effective plastic strain levels at (a) 0.021, (b) 0.10, (c) 0.20, and (d) 0.30 for the circular cylindrical specimen. An initial geometric defect was provided in the bottom right-hand corner, which acted as a trigger for the localization; note however that a necking mode is preferred here as opposed to a macroshear band.

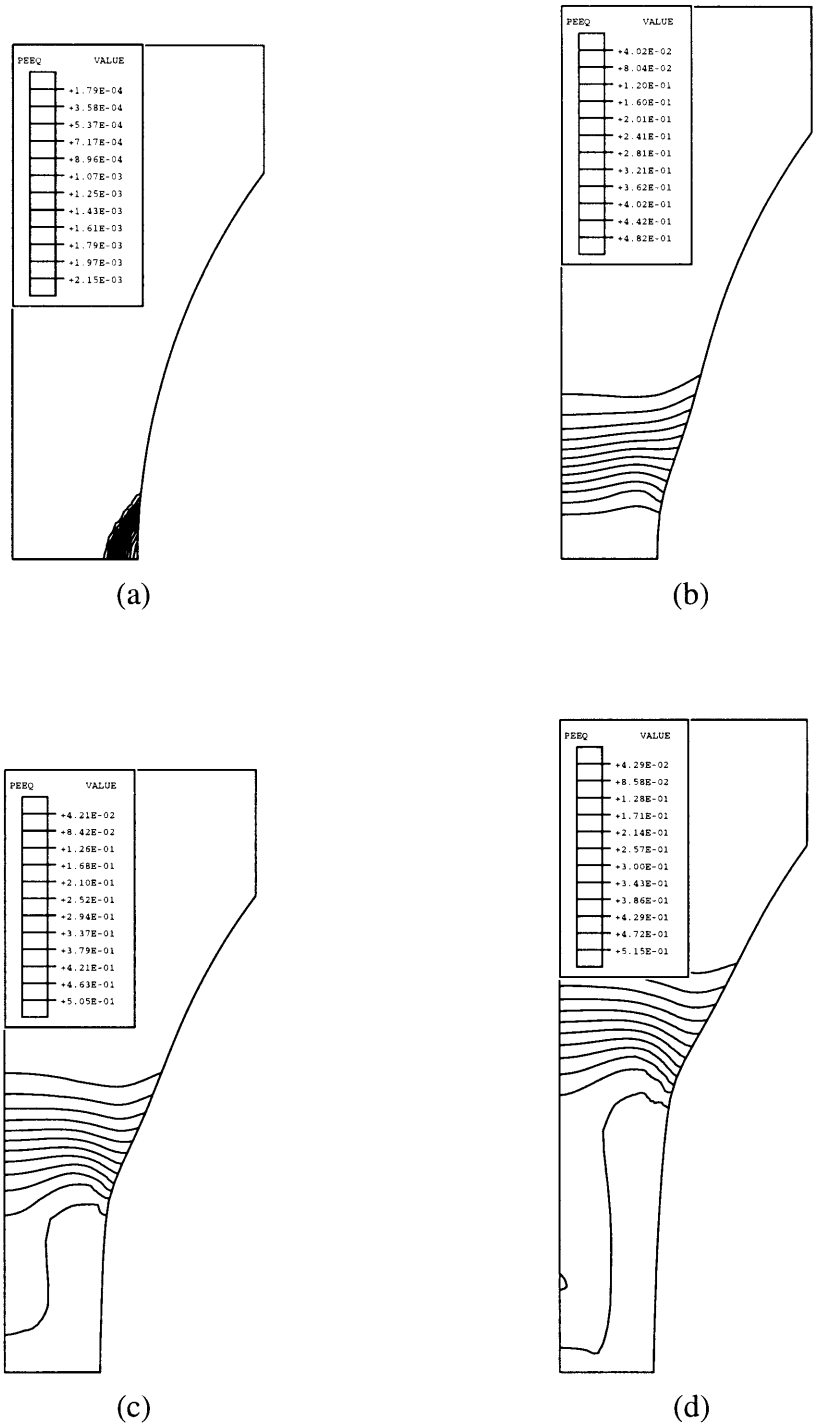

Fig. 18. The figures show the contours of constant effective plastic strain levels at (a) 0.0213, (b) 0.10, (c) 0.20, and (d) 0.30 for the hour-glass shaped specimen. Due to the inhomogeneous nature of the stress field in this specimen, an initial defect was not required to trigger the localization.

explicitly incorporated into the constitutive model. All of the qualitative observations of their experiments and numerical simulations are reproduced in the present simulation, but without introducing intrinsic material softening.

5. Figures 19 and 20 show the σ_{22} contours in both types of specimens. Clearly, the stress field is not uniform, even in the fully stretched region; the pointwise variation of the true stress at the minimum cross-section at 30% global nominal strain is shown in Fig. 21. In experimental investigations with these types of specimens, typically the applied load and the diameter are measured to determine an average true stress. The result in Fig. 21 indicates that interpretation of the experimental results in terms of the average stress over the minimum cross-section is likely to lead to errors in interpretation of the constitutive behavior of the material. We explore this further in both the cylindrical and hour-glass shaped specimens.
6. The growth of the localization is quite sensitive to the aspect ratio of the specimen, as demonstrated already with the specimens with rectangular cross-section. Figure 22 shows the variation of the nominal stress with the global strain δ/L for L/R ratios of 2, 5 and 10. The load drop and localization appear more rapidly in the longer specimens, just as in the case of the rectangular specimens. Clearly, the loading rate and the material rate dependence will also have a significant effect on the overall tensile response of the specimens, but these have been suppressed in the simulations.
7. In experiments with circular cylindrical specimens, it is not possible to identify a priori the location of the neck formation; typically, experimental measurements of load and global elongation are converted to a true stress and true strain by assuming a constant volume deformation. Using this scheme, the load vs elongation plot determined from the numerical simulations can also be displayed as a 'true-stress vs true-strain' diagram. This numerically simulated stress stain curve is compared to the imposed trilinear stress–strain curve in Fig. 23. Clearly, near the peak-load, the discrepancy is quite large; in fact, the experimental interpretation shows a drop in the 'true stress' while the constitutive model assumed in the simulation was monotonically increasing.
8. In the case of the hour-glass shaped specimen, it is obvious that one obtains the structural response. The load vs diametral contraction data from such experiments are usually converted to a 'true-stress vs true strain' plot. The 'true stress' is obtained by normalizing the load by the current area; the 'true logarithmic strain' is calculated from the diametral contraction at the minimum cross section, assuming a constant volume deformation. Interpreting the load-elongation results of the numerical simulation shown in Fig. 16 in this manner results in the 'true-stress' vs 'true-strain' characterization shown in Fig. 24. Clearly, this is very different from the assumed trilinear constitutive description of the material, also shown in the figure. First, the slope of the elastic region is not the modulus of elasticity of the material, but the structural stiffness of the hour-glass shaped specimen. Second, the stress level at the onset of localization is significantly enhanced due the triaxial state of stress in this specimen; this level can be altered by adjusting the radius of curvature and the waist dimension of the hour-glass specimen. Finally, as the localization propagates along the length of the specimen, it encounters a much larger resistance than a cylindrical specimen since there does not exist a steady state neck growth regime in this specimen; in fact, the entire large deformation segment of the constitutive behavior must be obtained before the waist region reaches full stretch. The initial stiffness, the peak load, and the propagation load depend crucially on the geometrical parameters of this specimen. This

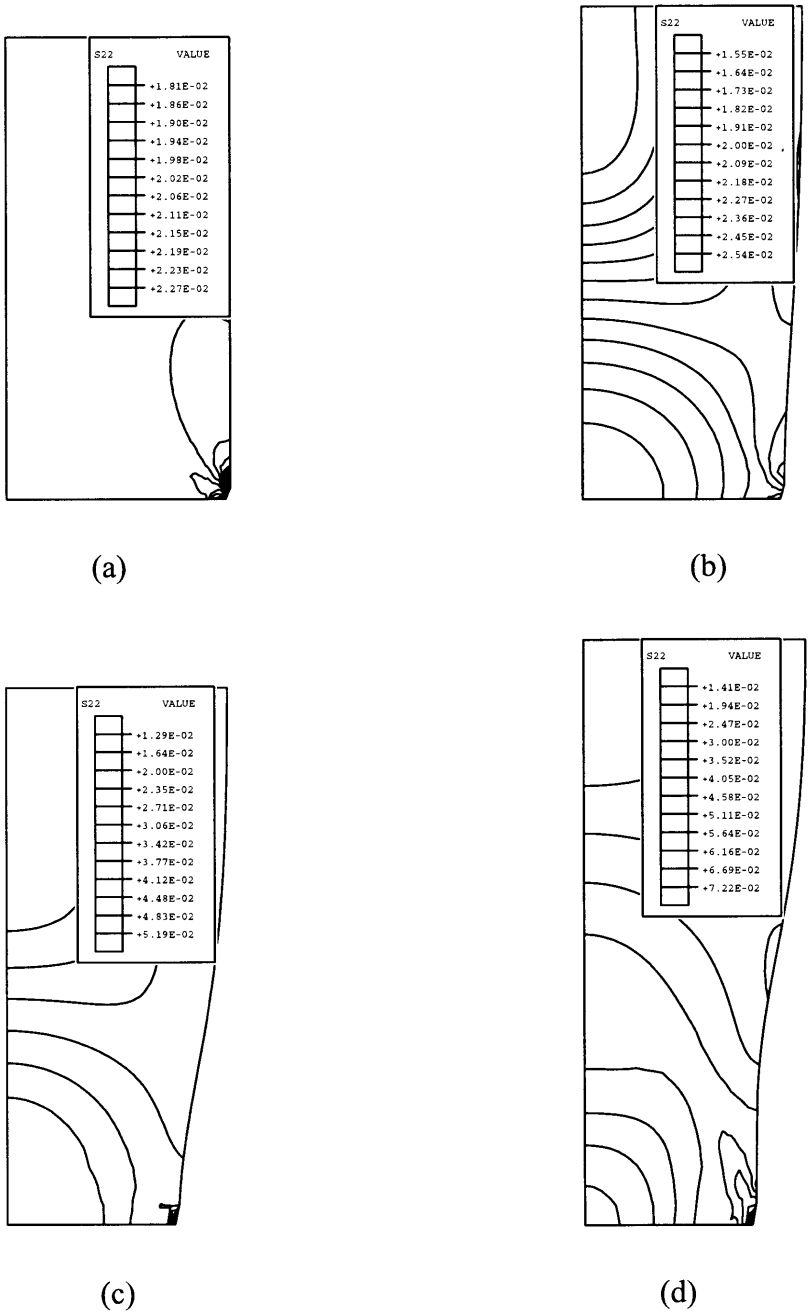

Fig. 19. The figures show contours of the normal stress σ_{22} at engineering strain levels at (a) 0.021, (b) 0.10, (c) 0.20, and (d) 0.30 for the circular cylindrical specimen. Note that the stress across the specimen cross-section is far from uniform.

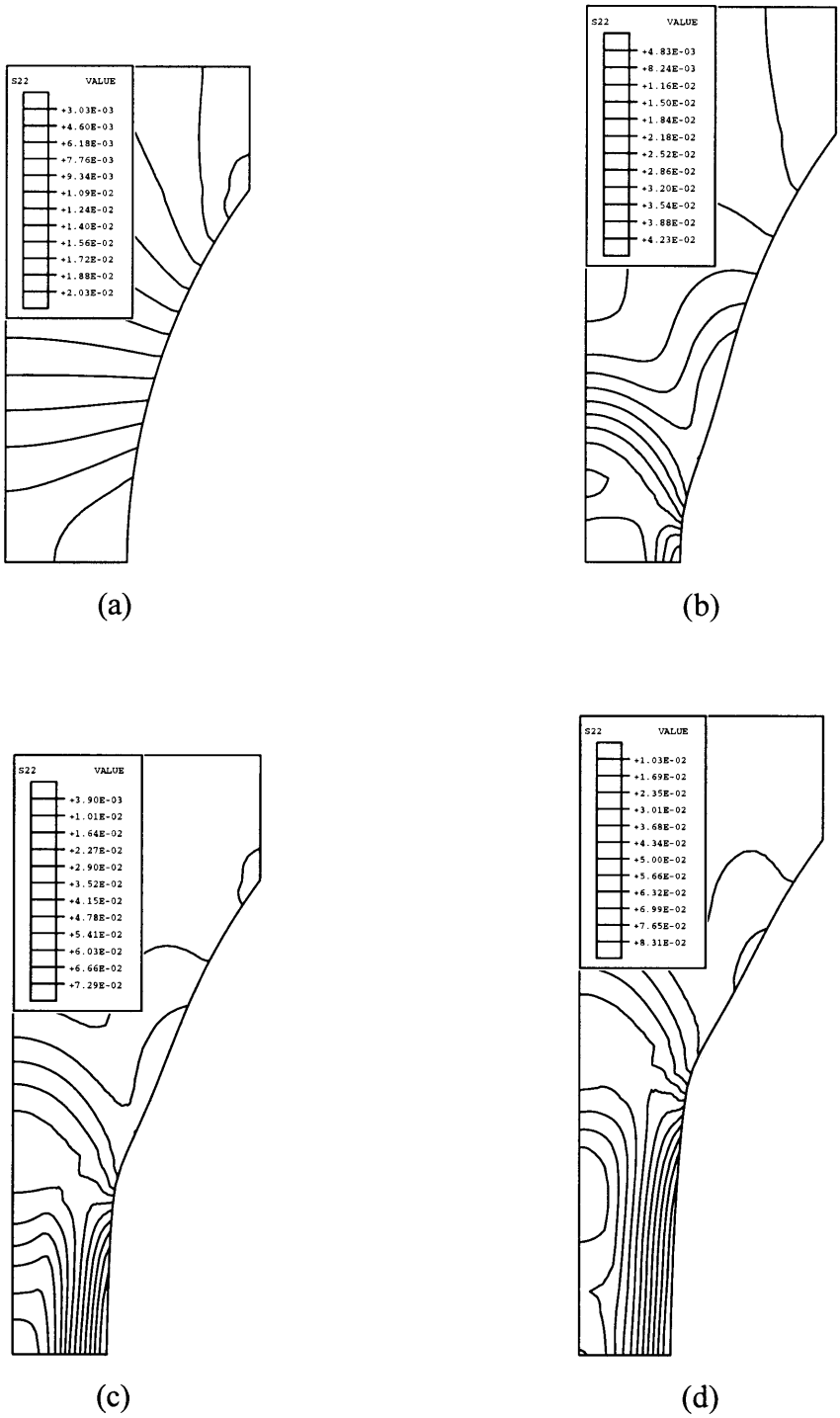

Fig. 20. The figures show contours of the normal stress σ_{22} at engineering strain levels at (a) 0.021, (b) 0.10, (c) 0.20, and (d) 0.30 for the hour-glass shaped specimen. Note that the stress across the specimen cross-section is far from uniform.

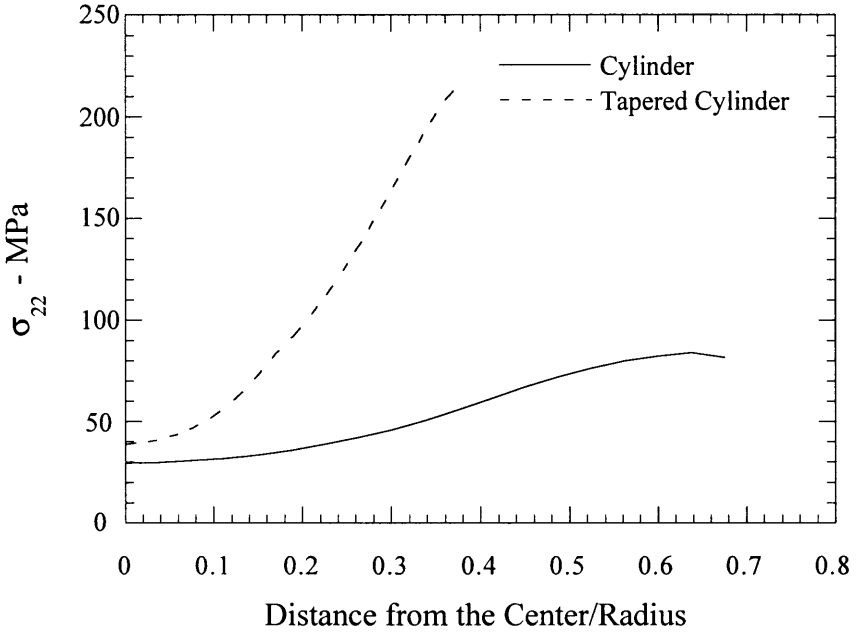

Fig. 21. Variation of the normal stress across the specimen in the circular cylindrical and the hour-glass shaped specimens at a global engineering strain level of 30%.

specimen may be designed to minimize the geometrical influences on the stiffness as well as the onset of localization, but the hour-glass specimen does not yield the constitutive properties of the material beyond the onset of localization at the waist.

In summary, the trilinear constitutive behavior assumed in this paper clearly reproduces the tensile response of the circular-cylindrical and the hour-glass shaped specimens. Of course, in all of the above simulations, rate and temperature dependence of the material have been excluded; we expect that incorporation of these influences as well as the onset of inelastic behavior well below the peak load in the tensile response will result in quantitative matching of experimental results while we have demonstrated qualitatively similar response.

5. Conclusion

The problem of localization of deformation in a class of shear yielding polymers was investigated. The conclusions of this investigation are listed below.

1. The phenomenon of shear banding, stabilization into a neck profile and steady-state neck propagation were shown to bear a striking resemblance to the phenomenon of Lüder's band formation and growth in metallic materials. This similarity is in spite of the fact that the underlying molecular/atomistic mechanisms of deformation are quite different, and suggests that one might model the shear banding phenomenon in polymers in a similar fashion to models of Lüder's bands in metal, i.e. using a continuum theory.

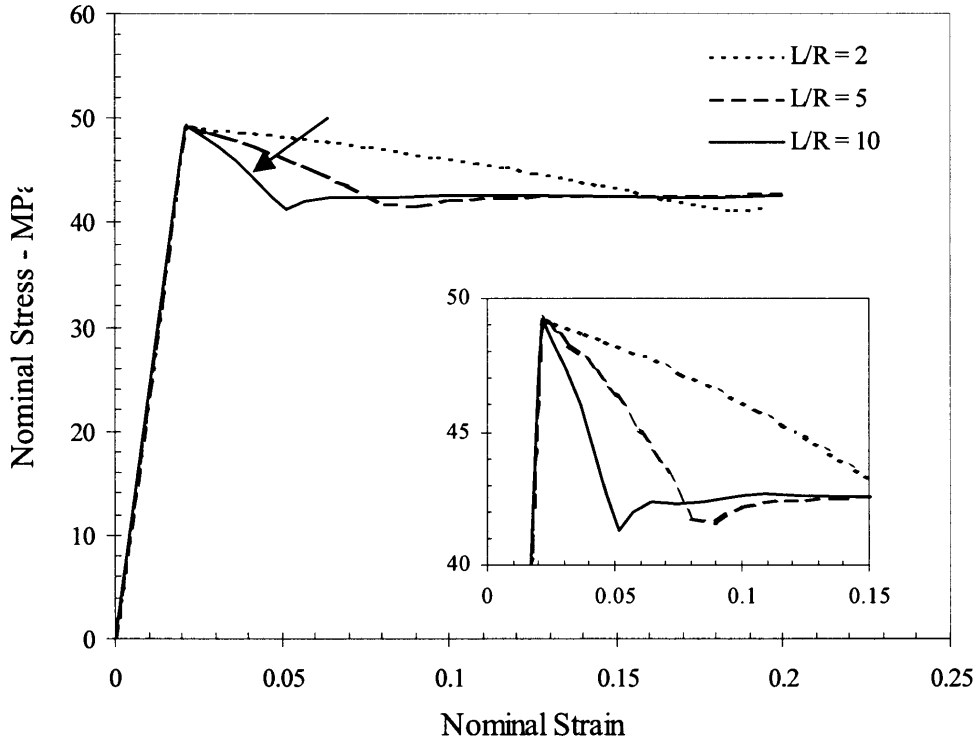

Fig. 22. Numerically stimulated tensile response of the circular cylindrical specimen, indicating the engineering stress-strain curve. The specimen aspect ratio influences the rapidity with which the localization sets in; this is indicated in the inset plot, where the region near the peak load is expanded.

2. A trilinear stress-strain equation is assumed to hold for polycarbonate, which is taken as one representative member of the class of shear yielding polymers. From a brief review of previous experimental work, it is suggested that intrinsic material softening need not be imposed on the constitutive description.
3. A numerical simulation of the shear banding initiation and growth is demonstrated using a trilinear material model incorporated into the commercial code ABAQUS. A full three-dimensional simulation was performed to model the details of the post-localization response. Reduced integration is needed only to provide a sharp band transition in a relatively coarse mesh.
4. Shear band localization is demonstrated in materials with a hardening behavior in the true-stress vs logarithmic strain relationship, demonstrating that intrinsic softening is not the driving force behind deformation localization in these materials.
5. The complete tensile response of uniaxial deformation in specimens with rectangular, circular cylindrical, and hour-glass shapes was obtained using numerical simulations and demonstrated to duplicate the experimentally observed tensile response. Interpreting the results of the numerical simulations in a manner typically used in experiments, it is shown that neither the circular cylindrical specimen, nor the hour-glass specimen can be used to determine the constitutive behavior experimentally at deformations beyond the onset of localization.

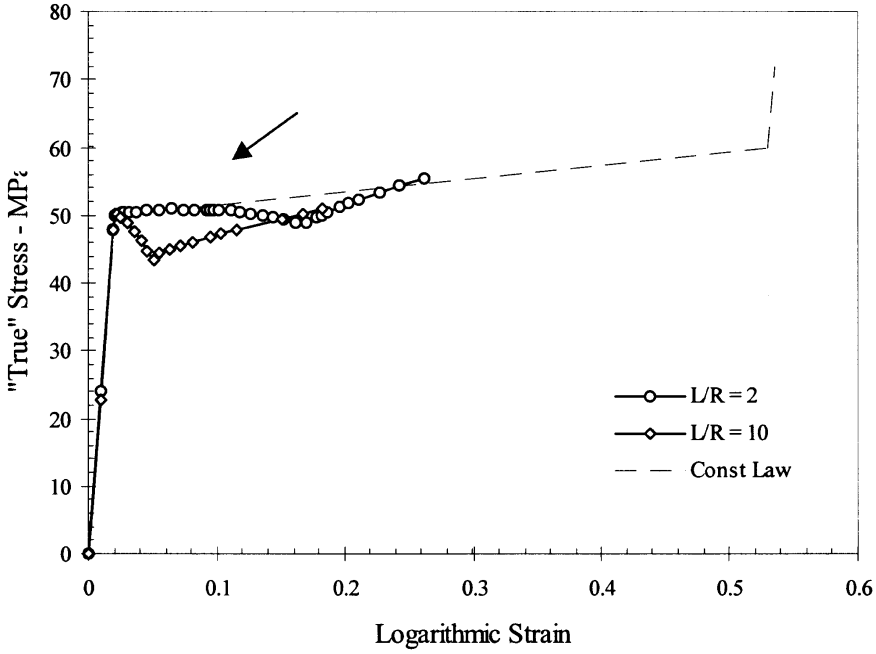

Fig. 23. 'True' stress vs logarithmic strain variation obtained from numerical simulation of circular cylindrical specimens compared with the assumed trilinear constitutive law. The post-peak load region exhibits a significant deviation from the constitutive law and this deviation is significantly influenced by the aspect ratio.

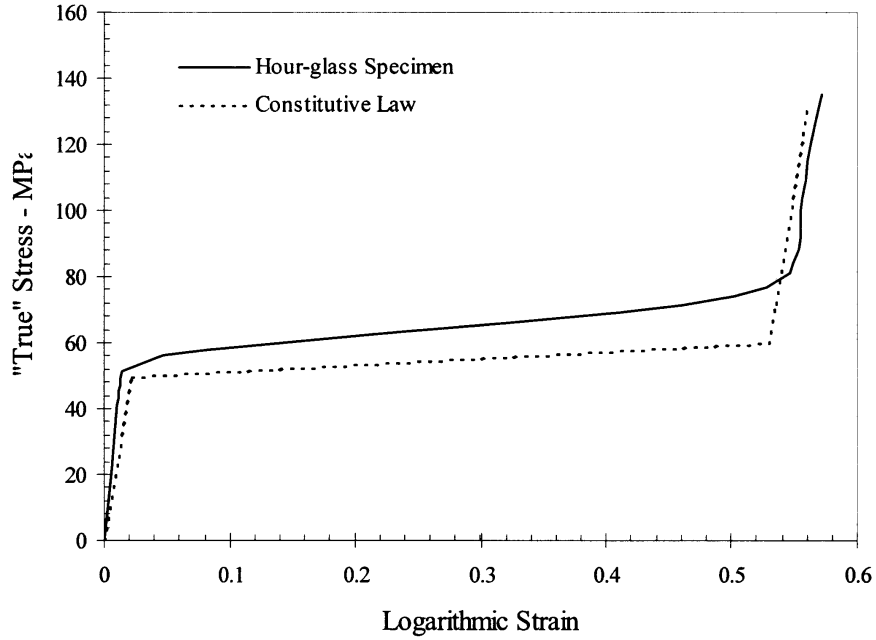

Fig. 24. 'True' stress vs logarithmic strain variation obtained from numerical simulation of an hour-glass shaped specimen compared with the assumed trilinear constitutive law. The initial slope and the peak load when localization begins are influenced significantly by the geometry of the hour-glass specimen.

A number of influences on the constitutive behavior have been ignored in the present work; in particular, pressure, temperature, and strain-rate dependence of the inelastic behavior were all suppressed in the present model. All of these conditions are important in governing inelastic deformation. Specifically, the appearance of localization can be suppressed by suitably altering the pressure, temperature, and strain rate. These issues will be addressed in a future contribution. We have also not explored shear deformations in this manuscript; in a sequel to this paper, we aim to describe an experimental and numerical characterization of predominantly shear loaded specimens.

References

Argon, A. S., 1973. A theory for the low-temperature plastic deformation of glassy polymers. Philosophical Magazine 28, 839–865.

Arruda, E. M., Boyce, M. C., 1993. Evolution of plastic anisotropy in amorphous polymers during finite straining. International Journal of Plasticity 9, 697–720.

Bowden, F. P., Raha, S., 1970. The formation of micro shear bands in polystyrene and polymethylmethacrylate. Philosophical Magazine 22, 463–482.

Boyce, M. C., Parks, D. M., Argon, A. S., 1988. Large inelastic deformation of glassy polymers. Part I: Rate dependent constitutive model. Mechanics of Materials 7, 15–33.

Boyce, M. C., Arruda, E. M., Jayachandran, R., 1994. The large strain compression, tension and simple shear of polycarbonate. Polymer Engineering and Science 34, 716–725.

Brown, N., Ekvall, R. A., 1962. Temperature dependence of the yield points in iron. Acta Metallurgica 10, 1101–1107.

Brown, N., Ward, I. M., 1968. Load drop at the upper yield point of a polymer. Journal of Polymer Science: Part A-2 6, 607–620.

Buisson, G., Ravi-Chandar, K., 1990. On the constitutive behavior of polycarbonate under large deformation. Polymer 31, 2071–2076.

Fager, L. O., Bassani, J. L., 1986. Plane strain neck propagation. International Journal of Solids and Structures 22, 1243–1257.

G'Sell, C., Jonas, J. J., 1979. Determination of the plastic behavior of solid polymers at constant true strain rate. Journal of Materials Science 14, 583–591.

G'Sell, C., Gopez, A. J., 1985. Plastic banding in glassy polycarbonate under plane simple shear. Journal of Materials Science 20, 3462–3478.

Hall, E. O., 1970. Yield point phenomena in metals and alloys. Plenum Press, New York.

Haward, R. N., Thackray, G., 1968. The use of a mathematical model to describe isothermal stress–strain curves in glassy polymers. Proceedings of the Royal Society of London A 302, 453–472.

Haward, R. N., 1973. Post-yield behavior of amorphous plastic. In: Haward, R. N. (Ed.), The Physics of Glassy Polymers. John Wiley and Sons, New York.

Hetenyi, M., 1952. A study in photoplasticity. Proceedings of the First National Congress in Applied Mechanics.

Hill, R., 1948. A theory of the yielding and flow of anisotrophic metals. Proceedings of the Royal Society of London A 193, 281–297.

Hutchinson, J. W., Neale, K. W., 1983. Neck propagation. Journal of Mechanics and Physics of Solids 31, 405–426.

Knauss, W. G., Emri, I., 1987. Volume change and the nonlinear thermo-viscoelastic constitution of polymers. Polymer Engineering and Science 27, 86–100.

Kyriakides, S., 1994. Propagating instabilities in structures. In Advances in Applied Mechanics, Vol. 30. Academic Press, New York, pp. 67–189.

Lomer, W. M., 1952. The yield phenomenon in polycrystalline mild steel. Journal of Mechanics and Physics of Solids 1, 64–73.

Mote, J. D., Tanaka, K., Dorn, J. E., 1961. Effect of temperature on yielding in single crystals of the hexagonal Ag–Al intermetallic phase. Transactions of the Metallurgical Society of AIME 221, 858–866.

Nadai, A., 1950. Theory of flow and fracture in solids, Vol. 1, 2nd ed. McGraw-Hill, New York.

Needleman, A., 1988. Material rate dependence and mesh sensitivity in localization problems. Computer Methods in Applied Mechanics and Engineering 67, 69–85.
Nemat-Nasser, S., 1989. Phenomenological modeling of rate-dependent plasticity for high strain rate problems. Mechanics of Materials 7, 319–344.
Ortiz, M., Leroy, Y., Needleman, A., 1987. A finite element method for localized failure analysis. Computer Methods in Applied Mechanics and Engineering 61, 189–214.
Shaw, J. A., Kyriakides, S., 1996. Initiation and propagation of localized deformation in elasto-plastic strips under uniaxial tension. EMRL Report No. 96/10, University of Texas at Austin.
Thomas, T. Y., 1961. Plastic flow and fracture in solids. Academic Press, New York.
Tugcu, P., Neale, K. W., 1987. Necking and neck propagation in polymeric materials under plane-strain tension. International Journal of Solids and Structures 23, 1063–1085.
Wu, P. D., van der Giessen, E., 1994. Analysis of shear band propagation in amorphous glassy polymers. International Journal of Solids and Structures 31, 1493–1517.
Wu, P. D., van der Giessen, E., 1995. On neck propagation in amorphous glassy polymers under plane strain tension. International Journal of Plasticity 11, 211–235.
Zbib, H. M., Jubran, J. S., 1992. Dynamic shear banding: A three-dimensional analysis. International Journal of Plasticity 8, 619–641.